



Advanced Materials for NH₃ Capture: Interaction Sites and Transport Pathways

Cite as

Nano-Micro Lett.

(2024) 16:228

Hai-Yan Jiang^{1,2}, Zao-Ming Wang⁴, Xue-Qi Sun¹, Shao-Juan Zeng¹, Yang-Yang Guo¹,
Lu Bai^{1,2} ✉, Ming-Shui Yao^{1,2} ✉, Xiang-Ping Zhang^{1,2,3} ✉

Received: 2 February 2024

Accepted: 26 April 2024

© The Author(s) 2024

HIGHLIGHTS

- An overview of advanced materials for NH₃ capture from the aspects of interaction sites and transport pathways is presented.
- The classifications, working principles, design ideas and structure–property relationships on materials for NH₃ capture are discussed in detail.
- The challenges and encouraging outlooks with worthwhile directions for NH₃ capture are proposed.

ABSTRACT Ammonia (NH₃) is a carbon-free, hydrogen-rich chemical related to global food safety, clean energy, and environmental protection. As an essential technology for meeting the requirements raised by such issues, NH₃ capture has been intensively explored by researchers in both fundamental and applied fields. The four typical methods used are (1) solvent absorption by ionic liquids and their derivatives, (2) adsorption by porous solids, (3) ab-adsorption by porous liquids, and (4) membrane separation. Rooted in the development of advanced materials for NH₃ capture, we



conducted a coherent review of the design of different materials, mainly in the past 5 years, their interactions with NH₃ molecules and construction of transport pathways, as well as the structure–property relationship, with specific examples discussed. Finally, the challenges in current research and future worthwhile directions for NH₃ capture materials are proposed.

KEYWORDS Ammonia capture; Solvents; Porous solids; Porous liquids; Membranes

✉ Lu Bai, lbai1207@ipe.ac.cn; Ming-Shui Yao, msyao@ipe.ac.cn; Xiang-Ping Zhang, xpzhang@ipe.ac.cn

¹ Key Laboratory of Green Process and Engineering, State Key Laboratory of Mesoscience and Engineering, Beijing Key Laboratory of Ionic Liquids Clean Process, Institute of Process Engineering, Chinese Academy of Sciences, Beijing 100190, People's Republic of China

² School of Future Technology, University of Chinese Academy of Sciences, Beijing 100049, People's Republic of China

³ China University of Petroleum, Beijing 102249, People's Republic of China

⁴ Institute for Integrated Cell-Material Sciences (iCeMS), Kyoto University, Sakyo-Ku, YoshidaKyoto 606-8501, Japan

Published online: 27 June 2024



SHANGHAI JIAO TONG UNIVERSITY PRESS

Springer

Abbreviations

AA	Acetamide	2D/3D materials	Two/three-dimensional materials
ACs	Activated carbons	dodpdc	4,4'-Dihydroxybiphenyl-3,3'-dicarboxylic acid
[Bmim][SCN]	1-Butyl-3-methylimidazolium thiocyanate	[DBU-PEG][NTf ₂] ₂	8,8'-(3,6Dioxaoctane-1,8-diyl)bis(1,8Diazabicyclo[5.4.0]undec-7-en-8-ium)
[Bmim][NTf ₂]	1-Butyl-3-methylimidazolium bis(trifluoromethylsulfonyl)imide		bis(trifluoromethylsulfonyl)imide)
[Bmim][Zn ₂ Cl ₅]	1-Butyl-3-methylimidazolium chlorozincate	[DMEA][Ac]	N,N-dimethylethanolammonium acetate
[Bmim] ₂ [Co(NCS) ₄]	1-Butyl-3-methylimidazolium tetrakisothiocyanatocobaltate (II)	[EtOHim][NTf ₂]	1-Hydroxyethyl-3-methylbis(trifluoromethylsulfonyl)imide
[Bmim][MeSO ₃]	1-Butyl-3-methylimidazolium methanesulfonate	[EtOHim][BF ₄]	1-Hydroxyethyl-3-methyltetrafluoroborate
[Bmim] ₂ [CuCl ₄]	Bis(1-butyl-3-methylimidazolium) copper tetrachloride	[Emim][NTf ₂]	1-Ethyl-3-methylimidazolium bis(trifluoromethylsulfonyl)imide
[Bmim] ₂ [NiCl ₄]	Bis(1-butyl-3-methylimidazolium) nickel tetrachloride	[EtOHmim][NTf ₂]	1-(2-Hydroxyethyl)-3-methylimidazolium bis(trifluoromethylsulfonyl)imide
[Bmim] ₂ [SnCl ₄]	Bis(1-butyl-3-methylimidazolium) stannum tetrachloride		
[Bpy][NTf ₂]	N-butyl pyridinium bis(trifluoromethylsulfonyl)imide	[Emim][BF ₄]	1-Ethyl-3-methylimidazolium tetrafluoroborate
[BOHmim][Zn ₂ Cl ₅]	1-(4-Hydroxy-butyl)-3-methylimidazolium chlorozincate	[Emim][Ac]	1-Ethyl-3-methylimidazolium acetate
[Bim][NTf ₂]	1-Butylimidazolium bis(trifluoromethylsulfonyl)imide	[Emim][EtOSO ₃]	1-Ethyl-3-methylimidazolium ethylsulfate
BBTA	1H,5H-benzo(1,2d), (4,5-d')bistriazole	[Emim][SCN]	1-Ethyl-3-methylimidazolium thiocyanate
BTC	1,3,5-Benzenetricarboxylic acid	[EtOHim][SCN]	1-Hydroxyethyl-3-methylthiocyanate
BTDD	Bis(1H-1,2,3-triazolo[4,5-b],[4',5'-i])dibenzo[1,4]dioxin	[EtOHmim][BF ₄]	1-(2-Hydroxyethyl)-3-methylimidazolium tetrafluoroborate
CPMs	Crystalline porous materials	[Eim][Li(NTf ₂) ₂]	1-Ethylimidazolium lithium bi(bis(trifluoromethylsulfonyl)imide)
COFs	Covalent organic frameworks		
CIPMs	Conventional inorganic porous materials	[Emim] ₂ [Co(NCS) ₄]	1-Ethyl-3-methylimidazolium tetrakisothiocyanatocobaltate (II)
CHBs	Cooperative hydrogen bonds	EaCl	Ethylamine hydrochloride
ChCl	Choline chloride	EG	Ethylene glycol
CA	Cellulose acetate	[EtA][SCN]	Ethanolamine thiocyanate
COOH-MWCNTs	Carboxylic group functionalized multiple-wall carbon nanotubes	EGDMA	Ethylene glycol dimethacrylate
[choline][NTf ₂]	Choline bis(trifluoromethylsulfonyl)imide	ENIL	Encapsulated ionic liquid
		FPMD	First-principles molecular dynamics
[CAM][Cl]	Carbamide chloride	GCMC	Grand canonical Monte Carlo
DESs	Deep eutectic solvents		

Gly	Glycerol	PhO	Phenol
GI-POSS	Octaglycidyl polyhedral oligomeric silsesquioxane	PDAB-AA	Poly(divinylbenzene) acrylic acid
HBA	Hydrogen-bond acceptors	PIM-1-COOH	Polymers of Intrinsic Microporosity modified with carboxylic acid
HBD	Hydrogen-bond donors	PAA	Poly(amic acid)
HOF	Hydrogen bond frameworks	PDF	Pair distribution function
HS	Hollow silica	PB	Prussian blue
HTCS	High throughput computational screening	PPc	Polypthalocyanine
[Hmim][BF ₄]	1-Hexyl-3-methylimidazolium tetrafluoroborate	PDMS	Poly(dimethylsiloxane)
[Hmim] ₂ [Co(NCS) ₄]	1-Hexyl-3-methylimidazolium tetrakisothiocyanatocobaltate(II)	PVDF	Polyvinylidene difluoride
ILs	Ionic liquids	PEG	Polyethylene glycol
[Im][NO ₃]	Imidazolium nitrate	PIP	Porous ionic polymers
[Im][NTf ₂]	Imidazolium bis(trifluoromethylsulfonyl)imide	[P ₆₆₆₁₄][NTf ₂]	Trihexyl(tetradecyl)phosphonium bis(trifluoromethylsulfonyl)imide
[Li-TEG][NTf ₂]	Lithium triethylene glycol bis(trifluoromethylsulfonyl)imide	[Ph3ImH][NTf ₂] ₂	1,3,5-Tri(imidazolium-1-yl)bi(bis(trifluoromethylsulfonyl)imide)
MOPs	Metal-organic polyhedral	Res	Resorcinol
MOFs	Metal organic frameworks	SOMP	Sulfonated and ordered mesoporous polymer
MAA	N-methylacetamide	SCN	Thiocyanate
MMMs	Mixed matrix membranes	SILP	Supported ILs phase
[2-Mim][NTf ₂]	2-Methylimidazolium bis(trifluoromethylsulfonyl)imide	SAXS	Small-angle X-ray scattering
[2-Mim][Li(NTf ₂) ₂]	2-Methylimidazolium lithium bi(bis(trifluoromethylsulfonyl)imide)	TEG	Triethylene glycol
[MTEOA][MeOSO ₃]	Tris(2-hydroxyethyl)methylammonium methylsulfate	TA	Cobaltous thiocyanate
[MeOHim][NTf ₂]	1-Hydroxymethyl-3-methyl bis(trifluoromethylsulfonyl)imide	[1, 2, 3-TrizH ₂][NO ₃] ₂	1, 2, 3-Triazolium nitrate
[Me ₂ C ₂ ^{OH} N]Cl/	Dimethyl-di(2-hydroxyethyl) ammonium chloride	[1, 2, 3-TrizH ₂][CF ₃ SO ₃] ₂	1, 2, 3-Triazolium trifluoromethane sulfonate
[MeC ₃ ^{OH} N]Cl	Methyl-tri(2-hydroxyethyl) ammonium chloride		
NA	Nicotinate		
NIR	Near infrared spectroscopy		
NMR	Nuclear magnetic resonance		
OS	Organosilane		
[Omim][BF ₄]	1-Octyl-3-Methylimidazolium tetrafluoroborate		
PLs	Porous liquids		
PM2.5	2.5-Micrometer particulate matter		
POPs	Porous organic polymers		

1 Introduction

Ammonia (NH₃), an important basic chemical, is a feed stock for nitrogenous fertilizer production via the Haber process, which is important for global food safety [1–3]. It is also a promising clean energy source owing to its high hydrogen density and carbon-free nature, and it provides safer transport and storage compared with H₂ due to its easy liquefaction and low penetration rate toward transport equipment [4–8]. However, NH₃ is a toxic and irritating gas that is detrimental to human health. Specifically, it injures the human eyes, skin, respiratory tract, and liver when its concentration in the blood is higher than 25 ppm [9]. Meanwhile, the excessive emission of NH₃ in the atmosphere will participate in chemical reactions to



form 2.5- μm particulate matter (PM_{2.5}), causing negative effects such as haze and soil acidification, etc. [10, 11].

NH_3 -containing gases come from a wide range of sources. For example, it is inevitable to generate a large amount of NH_3 -containing exhausted gas during urea manufacturing and ammonia synthesis processes. In addition to the mentioned chemical process, the direct NH_3 emission from agriculture such as compost and animal breed place also causes serious negative effects [11, 12]. Therefore, NH_3 capture and recovery from these sources benefit both resource utilization and environmental protection. The traditional technologies for capturing NH_3 involve physical condensation and water/acid scrubbing. Physical condensation relies on a boiling point difference to achieve separation. In such a case, NH_3 -containing gas should be cooled to a lower temperature (e.g., $-15\text{ }^\circ\text{C}$) to liquify gaseous NH_3 , while other compounds remain gaseous, which always consumes more energy. Water/acid scrubbing depends on the different solubilities of gases in liquid solvents to achieve gas separation. However, the NH_3 recovery from water is energy-intensive, and large quantities of NH_3 -containing wastewater are inevitably produced, causing serious secondary pollution. Inorganic acid solutions, such as H_2SO_4 and H_3PO_4 are highly corrosive, and the reaction of inorganic acids with NH_3 is almost irreversible and generates the low-valued salts.

Based on the above analysis, it is necessary to develop novel green technologies for NH_3 capture and recovery, in which the design and controllable fabrication of advanced materials are crucial. To date, many materials have been developed, including ionic liquids (ILs), crystalline porous materials (CPMs), porous organic polymers (POPs), and their composites. However, most reviews have focused on a single topic such as ILs for NH_3 absorption [13–15] or metal–organic frameworks (MOFs) for NH_3 adsorption [16–19]. Overall reviews of both developed and emerging NH_3 capture materials are still limited. Rooted in the development of the advanced materials for NH_3 capture, we aimed to provide a coherent review of the design of different materials mainly over the past 5 years, and their interactions with NH_3 molecules, and the construction of transport pathways. This review first presents a summary of the categories of materials, including functional solvents, porous solids, porous liquids and emerging membranes, along with brief working principles and evaluated parameters. Then, the recent advancements in such materials are briefly reviewed in detail. Functional solvents including ILs and deep eutectic

solvents (DESSs), have been introduced due to their structural tunability, negligible vapor pressure, and lower energy consumption compared with traditional solvents. As for various NH_3 -containing gases separation system, balancing the absorption–desorption ability, costs, and variations in physical properties of functional solvents is challenging. As an alternative strategy, porous solids involving conventional inorganic porous materials (CIPMs), porous organic polymers (POPs), crystalline porous materials (CPMs), and composite adsorbents have been proposed, and their performances have been analyzed based on the pore properties and type of interaction sites. Such solids are difficult to be implemented in conventional flow processes, and their performance remains limited. And most of them faced with the problem of structural collapse. Based on the fluidity of liquid absorbents and the porosity of porous solids, an important direction for porous liquids (PLs) for NH_3 ab-adsorption was proposed. However, this technology is on the rise and not yet mature and requires to further development. Emerging organic, inorganic and hybrid membranes for NH_3 separation and their gas separation performance are discussed; however, it is difficult to meet the demands of industrialization, and the long-term stability of various membranes has still not been explored. In the conclusions and prospects of this review, challenges in current research and encouraging outlooks for the future application of such materials in advanced NH_3 capture are analyzed and proposed.

2 Working Principles

The design and development of these materials are important for achieving efficient NH_3 capture. Excellent NH_3 -capturing materials require two features. One is rich specific sites that can interact with NH_3 molecules to attain high affinity. It should be noted that the interaction cannot be too strong; otherwise, it is not conducive to the release of captured NH_3 from the materials. The other is the introduction of transport pathways, which are expected to provide modulable diffusion channels and rich accessible sites, thereby improving the NH_3 capture performance and reducing regeneration consumption.

According to the material characteristics and capture principle, the NH_3 capture materials can be divided into the following four types as shown in Fig. 1: absorbents (functional solvents, Sect. 3), adsorbents (porous solids, Sect. 4),

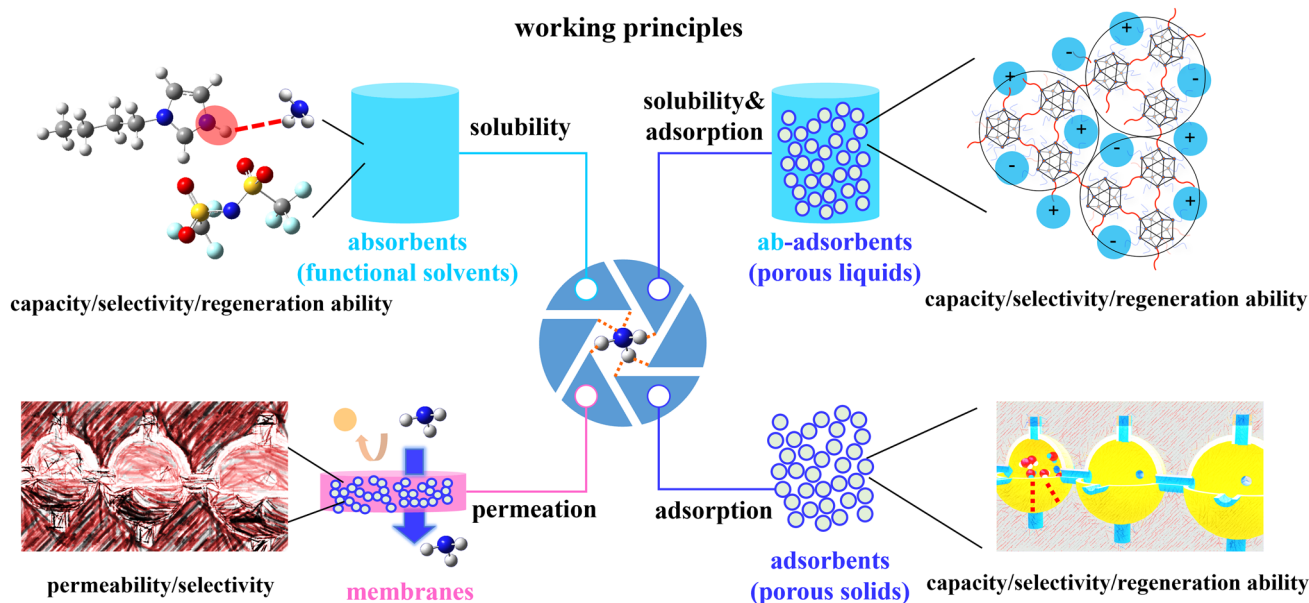


Fig. 1 Working principles of NH_3 capture materials

ab-adsorbents (porous liquids, Sect. 5), and membrane materials (Sect. 6).

Functional solvents utilize gas with different solubilities in liquid solvents to achieve selective NH_3 absorption. The interaction sites (hydroxyl groups, acidic protons, amino groups, metal ions, etc.) on functional solvents play an important role in enhancing the NH_3 absorption performance. The NH_3 absorption capacity of a given solvent, which is largely influenced by the pressure and temperature, can be determined by the gravimetric methods, vapor–liquid equilibrium apparatus, etc. [20, 21]. The regeneration ability of absorbents is another important evaluation parameter that is significantly related to the energy efficiency and economic benefits in practical applications.

The working principle of porous solids relies mainly on their confined micropores to accommodate gas molecules and the interaction sites in these pores to achieve selective NH_3 adsorption. The pore structures and interaction site strengths of porous solids can be obtained using a physical adsorption apparatus, temperature-programmed desorption of ammonia, and other methods. The NH_3 adsorption isotherm is normally measured using a gas adsorption instrument that monitors the change in pressure of a sample held at a given temperature when exposed to different ammonia pressures [22]. The NH_3 adsorption dynamics of samples can be investigated either by breakthrough curves [16],

which record the concentration curve of each component over time through a breakthrough column, or by dynamic mode measured on a gas adsorption instrument [23], which can provide the speed to reach equilibrium and the time-dependent adsorption capacity at a given pressure and temperature.

Although porous solids offer major benefits, such as lower energy penalties in adsorption–desorption cycles, they are difficult to implement in conventional flow processes. To address this limitation, ab-adsorbents, i.e., PLs, have been developed by introducing permanent porosity into liquid materials. The existence of intrinsic micropores in PLs allows for rapid NH_3 adsorption–desorption (kinetics) while maintaining liquid fluidity and high adsorption capacity and selectivity (thermodynamics) resulting from both components. Such a combination is also beneficial for reducing the regeneration consumption and thus increasing the energy efficiency compared with liquid absorption, owing to the introduction of a pore structure on the feasible gas diffusion pathways [24]. The gas uptake of PLs can be measured by gas adsorption equipment [25] and column breakthrough tests [26]. Annihilation lifetime spectroscopy (PALS) and density measurements [27, 28] are usually used to confirm the permanent porosity of PLs.

Membrane separation uses different gas permeation rates through membranes to achieve NH_3 selective separation.

Gas permeation tests usually use the differential pressure method; specifically, they can be divided into the constant pressure-variable volume and constant volume-variable pressure methods. Permeance and selectivity are key parameters for gas separation membranes [29, 30]. The permeance (P_i) and separation selectivity ($\alpha_{i/j}$) can be calculated using the following equations:

$$P_i = \frac{Q_i}{A\Delta p_i} \quad (1)$$

$$\alpha_{i/j} = \frac{P_i}{P_j} \quad (2)$$

where P_i and P_j represent the permeance of gases i and j , respectively ($\text{cm}^3 \text{ (STP)}/(\text{cm}^2 \text{ s cm Hg})$); $1 \text{ GPU} = 1 \times 10^{-6} \text{ cm}^3 \text{ (STP)}/(\text{cm}^2 \text{ s cm Hg})$; Q_i denotes permeate flow rate of gas i at the standard state ($\text{cm}^3 \text{ (STP) s}^{-1}$); and A and Δp_i represent the effective membrane area (cm^2) and transmembrane pressure difference of gas i , respectively.

3 Functional Solvents for NH_3 Absorption

As advanced solvents, ionic liquids (ILs) are prospective candidates for NH_3 capture. ILs are entirely composed of organic cations and organic/inorganic anions, which make them designable according to application requirements [13–15]. In addition, the unique properties of ILs, including negligible vapor pressure, low specific heat capacity, and excellent recyclability, greatly reduce the regeneration

energy consumption and solvent loss during the NH_3 capture process compared to water scrubbing [15, 31]. Current research on NH_3 capture using IL-based solvents involves the design and development of absorbents, mass-transfer investigation, process simulation and assessment, and industrial applications. The development of task-specific absorbents for efficient and reversible NH_3 capture is fundamental and critical; thus, it has attracted the attention of many researchers. In this section, the NH_3 absorption–desorption performance, physical property variation, and absorption mechanism of task-specific ILs and their analogous DESs are briefly discussed from the perspective of the types and numbers of interaction sites for NH_3 absorption (Fig. 2).

3.1 Task-Specific Ionic Liquids

Considerable efforts have been devoted to designing novel task-specific ILs for efficient NH_3 absorption. The interaction sites between ILs and NH_3 molecules play an important role in efficient and reversible NH_3 absorption. The introduction of hydroxyl groups, acidic protons, amino groups, sulfo-/carboxyl groups, and metal ions remarkably improves the NH_3 absorption capacity of ILs. Table 1 lists the NH_3 absorption capacities of representative ILs.

The dissolution behavior of NH_3 in conventional ILs was firstly reported in 2007, and it was inferred that strong intermolecular complexes between NH_3 and ILs are formed [32]. Subsequently, it was found that cations had a greater

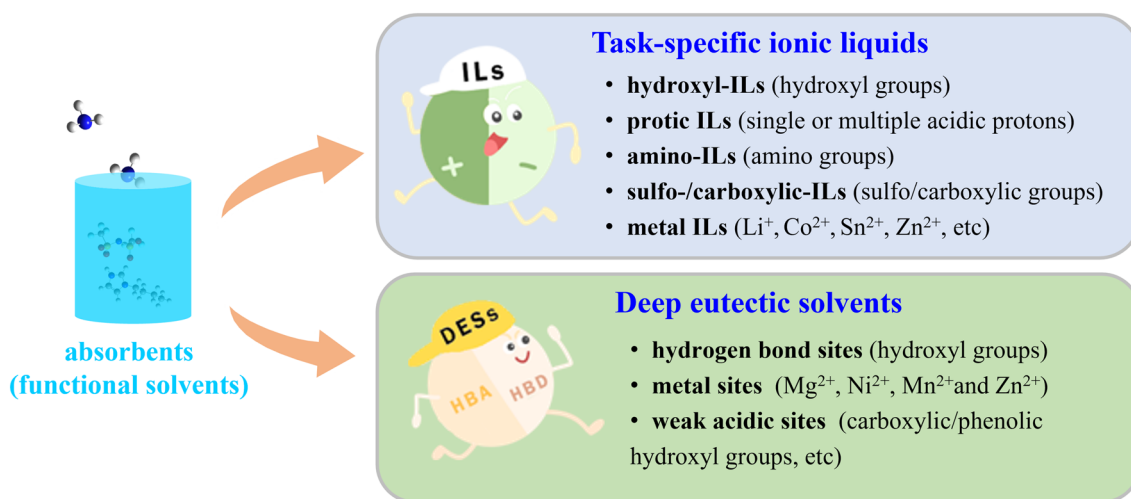


Fig. 2 Interaction sites on functional solvents for NH_3 absorption

Table 1 NH₃ absorption capacity of representative ILs

ILs	<i>T</i> (K)	<i>P</i> (kPa)	NH ₃ absorption capacity		References
			(mol NH ₃ /mol IL)	(mg NH ₃ /g IL)	
[Emim][BF ₄]	298	140	0.282	24	[34]
[Hmim][BF ₄]	298	220	0.485	32	[34]
[Omim][BF ₄]	298	120	0.389	23	[34]
[Bmim][SCN]	303	145	0.320	28	[34]
[Bmim][NTf ₂]	313	101	0.280	11	[38]
[Emim][Ac]	298.2	463	1.506	151	[32]
[Emim][EtOSO ₃]	298.1	421	1.075	77	[32]
[Emim][SCN]	298.1	307	0.799	80	[32]
[Bim][NTf ₂]	313	101	2.690	113	[38]
[Choline][NTf ₂]	293	100	1.857	82	[34]
[MTEOA][MeOSO ₃]	293	101	3.545	232	[35]
[DMEA][Ac]	298.1	278	1.604	183	[32]
[EtOHmim][NTf ₂]	313	128	0.830	35	[36]
[EtOHim][NTf ₂]	313	100	3.110	135	[21]
[EtOHim][BF ₄]	313	100	2.470	210	[21]
[EtOHim][SCN]	313	100	2.230	222	[21]
[MeOHim][NTf ₂]	313	100	3.040	136	[21]
[2-Mim][NTf ₂]	313	101	3.037	142	[41]
[Im][NTf ₂]	313	101	3.461	169	[41]
[1, 2, 3-TrizH ₂][NO ₃] ₂	313	101	4.187	365	[20]
[Eim][Li(NTf ₂) ₂]	313	101	6.618	169	[41]
[2-Mim][Li(NTf ₂) ₂]	313	101	7.012	183	[41]
[EtA][SCN]	293	101	2.538	359	[45]
[Bmim][Zn ₂ Cl ₅]	323	103.5	8.025	305	[47]
[Emim] ₂ [Co(NCS) ₄]	303	101	5.990	178	[49]
[Bmim] ₂ [Co(NCS) ₄]	303	101	6.030	163	[49]
[Hmim] ₂ [Co(NCS) ₄]	303	101	6.090	151	[49]
[Bmim] ₂ [CuCl ₄]	303	101	4.611	172	[50]
[Bmim] ₂ [NiCl ₄]	343	101	4.559	195	[50]
[Bmim] ₂ [SnCl ₄]	303	101	5.169	108	[50]
[Li-TEG][NTf ₂]	313	102.5	3.36	131	[51]

influence on NH₃ solubility than anions and that the hydrogen bond between the acidic 2-H of the imidazole cation and N atom of NH₃ played a crucial role in NH₃ absorption [33]. Thus, a feasible strategy for designing task-specific ILs is to tune the hydrogen-donating ability of the cations by adjusting the type and number of functional groups.

A series of task-specific ILs based on the hydrogen bond interaction were developed by introducing single hydroxyl functional groups and acidic protons into cations of ILs, and these ILs usually have higher NH₃ absorption capacity (0.83–4.2 mol NH₃/mol IL) than that of conventional ILs (<0.8 mol NH₃/mol IL), simultaneously showing great regeneration ability. Palomar et al. [34, 35] adopted the

COSMO-RS calculation method to screen potential NH₃ absorbents from 272 ILs and found that hydroxyl-functionalized ILs [EtOHmim][BF₄] and [choline][NTf₂] are promising for NH₃ absorption. As expected, a higher absorption capacity was achieved by hydroxyl-functionalized ILs compared with conventional ILs, and the separation mechanism of hydrogen bond interactions between ILs and NH₃ was further proved by near-infrared spectroscopy (NIR) and nuclear magnetic resonance (NMR) spectroscopy [36, 37]. Shang et al. [38] proposed a new strategy for introducing an acidic proton onto a cation to improve the NH₃ absorption capacity. The protic ionic liquid (PIL) [Bim][NTf₂] (Fig. 3a) exhibited high NH₃ absorption capacity with a value of 2.69 mol NH₃/

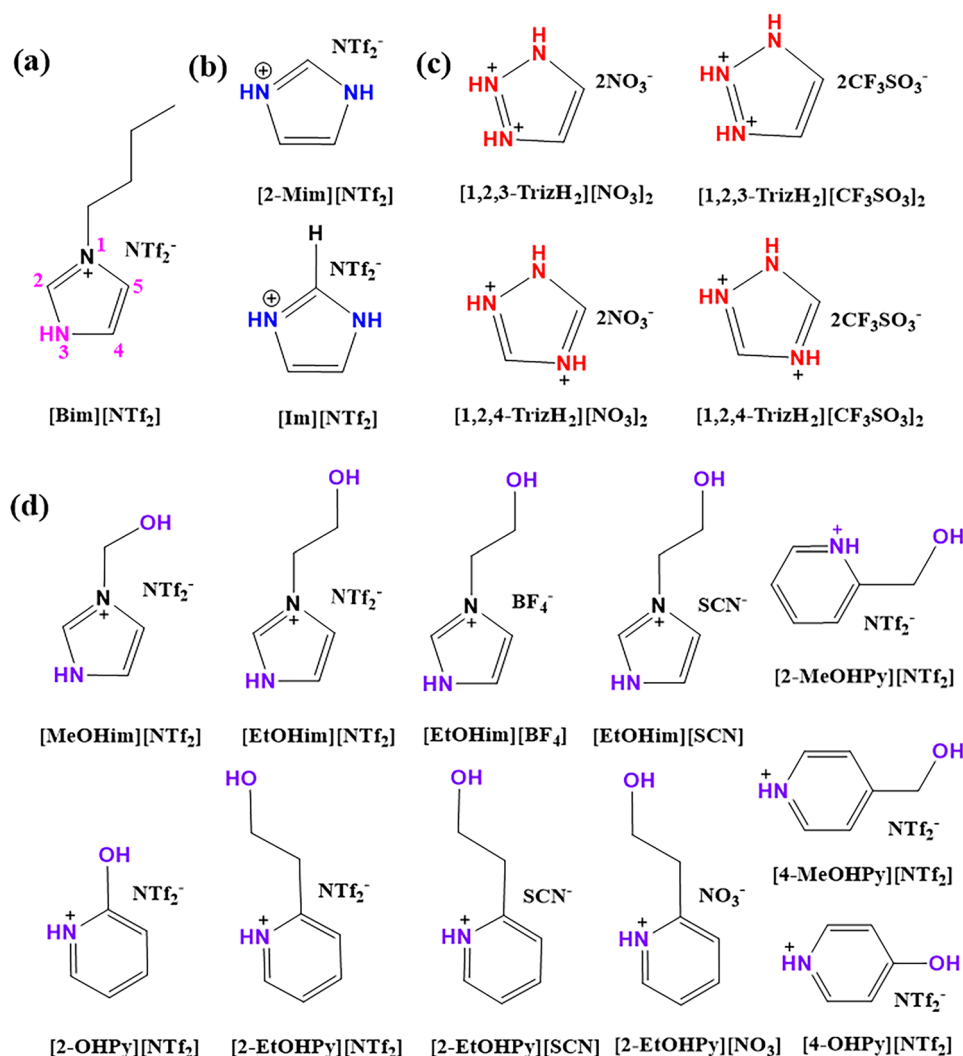


Fig. 3 a Structures of [Bim][NTf₂] [38]. b [2-Mim][NTf₂] and [Im][NTf₂] [41]. c Triazole cation-functionalized ILs [20]. d Dual-functionalized protic ILs [21, 42]

mol IL at 313 K and 100 kPa. There was no evident decline in the absorption ability of the recycled [Bim][NTf₂] after being used four times. Notably, the viscosity of the IL–NH₃ system during the NH₃ absorption process first increased and then decreased sharply to a lower value [39], which is completely different from the increased viscosity caused by CO₂ absorption. Furthermore, the NH₃ absorption mechanism of ILs was revealed through molecular dynamics (MD) simulations [40]. The results indicated that the energy of strong N3–H...N(NH₃) hydrogen bond between [Bim]⁺ and NH₃ molecules is up to $-79.0 \text{ kJ mol}^{-1}$, which is twice as strong as the hydrogen bond energy between C2–H of [Bmim]⁺ and NH₃. This strong interaction induced the enrichment of

cations at the PIL–gas interface, resulting in NH₃ molecules penetrating deeply into the bulk of the PILs and achieving selective absorption of NH₃ from gases containing N₂ and H₂. Besides, there are always other gases present, such as water in NH₃-containing gases in industrial streams. Trace water was also found to enhance NH₃ absorption owing to the cooperative absorption caused by [Bim][NTf₂] and H₂O.

Multiple hydrogen sites can be incorporated into the cations of ILs to improve their absorption performance through cooperative hydrogen bonding interactions. The NH₃ absorption capacity of imidazole-based ILs ([2-Mim][NTf₂] and [Im][NTf₂]) (Fig. 3b) with two acidic protons on cations was up to 3.46 mol NH₃/mol IL. The NH₃ absorption

capacity remained stable after five cycles of absorption and desorption [41]. Subsequently, Sun et al. [20] synthesized triazole cation-functionalized ionic liquids (TCFILs) containing three acidic protons (Fig. 3c). These TCFILs showed a rapid transition from the initial solid to liquid state during the NH_3 absorption process. Moreover, [1, 2, 3-TrizH₂][NO₃]₂ exhibited an ultrahigh NH_3 absorption capacity of 4.187 mol NH_3 /mol IL (about 365 mg NH_3 /g IL) at 303.15 K and 101 kPa and great recyclability benefiting from multiple hydrogen bonds, which is comparable to that of traditional water absorbents used in industry (300 mg NH_3 /g H₂O at 313 K and 101 kPa). Meanwhile, [1, 2, 3-TrizH₂][CF₃SO₃]₂ showed faster absorption kinetics than that of [1, 2, 3-TrizH₂][NO₃]₂. At the same time, the effect of water molecules on NH_3 absorption performance was studied. The results indicated that the addition of small amounts of water to [1, 2, 3-TrizH₂][CF₃SO₃]₂ had no obvious impact on the NH_3 capacity and shortened the absorption equilibrium time from 20 to 15 min, owing to the reduced viscosity of the systems. Additionally, simultaneously embedding acidic protons and hydroxyl groups on the cations of ILs is an efficient strategy to further improve NH_3 absorption capacity. Yuan et al. [21, 42] found that these imidazole- and pyridinium-based dual-functionalized PILs (DPILs) (Fig. 3d) possessed higher NH_3 solubility than ILs functionalized only by a single hydroxyl group. Specifically, the NH_3 solubility

of [EtOHim][NTf₂] was as high as 3.110 mol NH_3 /mol IL, which is approximately 30-fold greater than that of [Emim][NTf₂] and four-fold greater than that of the functionalized IL [EtOHmim][NTf₂]. These DPILs also exhibited outstanding recyclability, an excellent NH_3 /CO₂ selectivity of 65, and NH_3 /N₂ selectivity of 104.

There have been a few reports on the application of amino-functionalized ILs for NH_3 absorption. For example, Luo et al. [43, 44] designed a series of cation-functional PILs with single or multiple amidino groups (Fig. 4). Reversible cooperative hydrogen bond (CHB) networks were formed by hydrogen bond interactions between ammonia and amidino groups. The NH_3 absorption–desorption process was accompanied by the breakage and reformation of CHBs in the ILs, which led to a sigmoidal NH_3 absorption isotherm and energy-saving desorption. The [BzAm][NTf₂] showed NH_3 absorption with a threshold pressure of 0.28 kPa and capacity of 2.8 mol NH_3 /mol IL at 100 kPa. The absorbed NH_3 could also be rapidly stripped at 323 K and 1 kPa within 30 min. In addition, the threshold pressure and NH_3 ammonia production capacity could be tuned by varying the CHB interactions in the ILs. Similarly, Deng et al. [45] synthesized six protic ethanolamine-based ILs with multiple binding sites for efficient and reversible NH_3 uptake. Among them, ethanolamine thiocyanate ([EtA][SCN]) had suitable viscosity of 78.18 mPa s and exhibited the best absorption

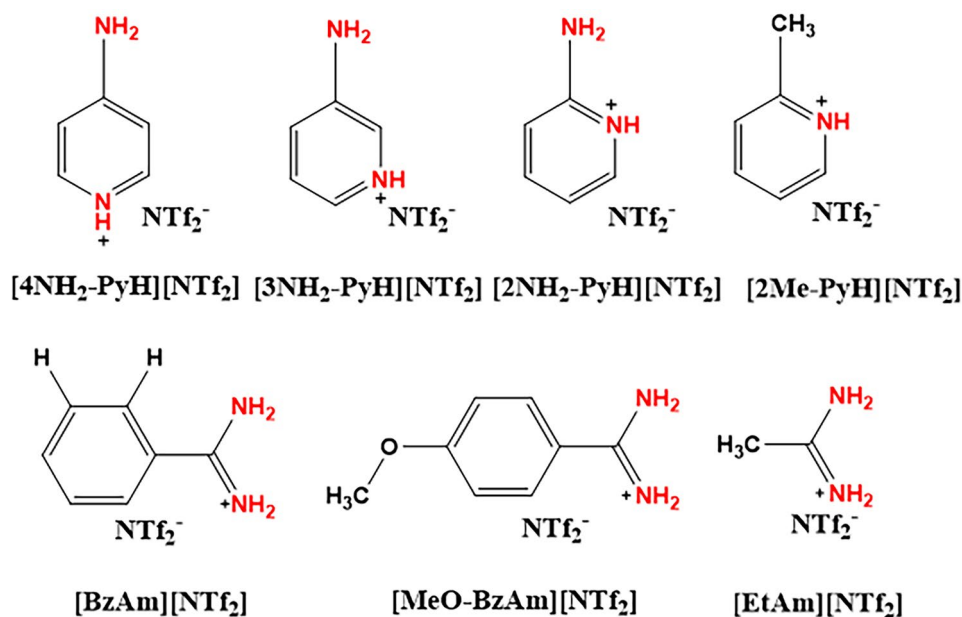


Fig. 4 Structures of cation-functional PILs with single or multiple amidino-groups [43, 44]

ability of 2.538 mol NH₃/mol IL at atmospheric pressure and 293.15 K due to multiple hydrogen-bonding interactions between acidic protons, hydroxyl groups, and thiocyanate with NH₃. In addition, the outstanding NH₃/CO₂ ideal selectivity with a value of 365 was observed in [EtA][SCN], which provides a competitive way to selectively separate NH₃ from CO₂ in tail gas.

At the same time, NH₃ is typically an alkaline gas. The introduction of Brønsted acidic groups to react with NH₃ is expected to improve the absorption capacity of ILs. Recent studies have shown that imidazolium- and ammonium-based ILs with sulfo and carboxy groups exhibit higher NH₃ solubilities than conventional and hydroxy-functionalized ILs. Moreover, the acidity of the Brønsted acidic group and the chemical structures of the acidic group and constituent ions also significantly affected the NH₃ capacity [46]. Another effective approach for improving the NH₃ absorption capacity is to develop metal ILs based on complexation with NH₃. Pioneering work on metal ILs for NH₃ absorption was reported in 2013, which used [Bmim][Zn₂Cl₅] as an NH₃ absorbents and showed a superior absorption capacity of 8.0 mol NH₃/mol IL at 323 K and 100 kPa, but the strong complex interaction between metal ILs and NH₃ molecules led to irreversibility of the materials [47, 48]. To solve the above problems, Zeng et al. [49] designed a series of novel cobalt ILs, [C_{*n*}mim]₂[Co(NCS)₄] (*n* = 2, 4, or 6), for reversible NH₃ absorption. The cobalt ILs exhibited a remarkable NH₃ absorption capacity of 6.09 mol NH₃/mol IL, which is more than 30 times higher than those of conventional ILs [C_{*n*}mim][SCN] without metals. This superior performance was attributed to the moderate Lewis acid–base interaction and cooperative hydrogen bonding between the MILs and NH₃ confirmed by experimental characterizations and density functional theory (DFT) calculations. At the same time, these cobalt ILs exhibited excellent recyclability and maintained a stable NH₃ capacity after five cycles. Wang et al. [50] further systematically studied the effects of various metal centers on the physicochemical properties and NH₃ absorption capacity. Among the range of MILs, [Bmim]₂[SnCl₄] not only showed a high absorption capacity of 5.169 mol NH₃/mol IL at 303.15 K and 100 kPa, which is much higher than that of conventional ILs, but also showed no obvious NH₃ capacity loss after five absorption and desorption cycles.

In addition to the above high-valence MILs, alkali metal ions, especially lithium (Li), have also been introduced into

PILs to increase NH₃ absorption performance. Shang et al. [41] prepared novel sorbents that simultaneously incorporate acidic protons into cations and Li⁺ ions into anions. The solid ILs gradually became liquids after NH₃ adsorption. An exceptional NH₃ capacity of 7.01 mol NH₃/mol IL was achieved using [2-Mim][Li(NTf₂)₂] at 313 K and atmospheric pressure, which is the highest NH₃ capacity reported for an IL to date. This superior capacity is attributed to the synergistic effect of hydrogen bonding between acidic protons and NH₃, as well as the Lewis acid–base interaction between the Li⁺-based anion and NH₃. Inspired by this, Cai et al. [51] further synthesized liquid chelation-activated multi-site ILs for reversible chemical absorption of NH₃, as shown in Fig. 5. The chelation of triethylene glycol (TEG) with Li⁺ activates the hydroxyl sites in TEG for strong interaction with NH₃, resulting into an outstanding NH₃ absorption capacity of 3.36 mol NH₃/mol IL at 313 K and 102.5 kPa.

3.2 Deep Eutectic Solvents

Given the lone-pair electrons and alkalinity of NH₃, the DESs with strong hydrogen-bond donating ability or Brønsted acidity are usually useful for capturing NH₃. DESs generally consist of two or three components capable of intermolecular interactions, particularly hydrogen bond interactions, which have lower melting points than those of each separate component [52]. They can be easily prepared by simply mixing hydrogen bond acceptors (HBAs) with hydrogen bond donors (HBDs). The introduction of a second or third component effectively reduces the viscosity and improves the mass transfer efficiency. Because of the diverse structures of HBAs and HBDs, many DESs have been synthesized for NH₃ absorption. Table 2 lists the NH₃ absorption capacities of representative DESs.

The current interest in DESs for NH₃ absorption is rooted in the pioneering work on hybrid ternary DESs with flexible hydrogen-bonded supramolecular networks designed by Li et al. [53]. The reported DESs are composed of choline chloride (ChCl), resorcinol (Res), and glycerol (Gly), which break the trade-off between NH₃-DES interaction strength and the stability of traditional DESs. The NH₃ mass solubility of ChCl/Res/Gly (1:3:5) DESs reached 130 mg g⁻¹ at 313 K and 101 kPa, which exceeds those of hydroxyl-functionalized ILs and ordinary DESs. More importantly,

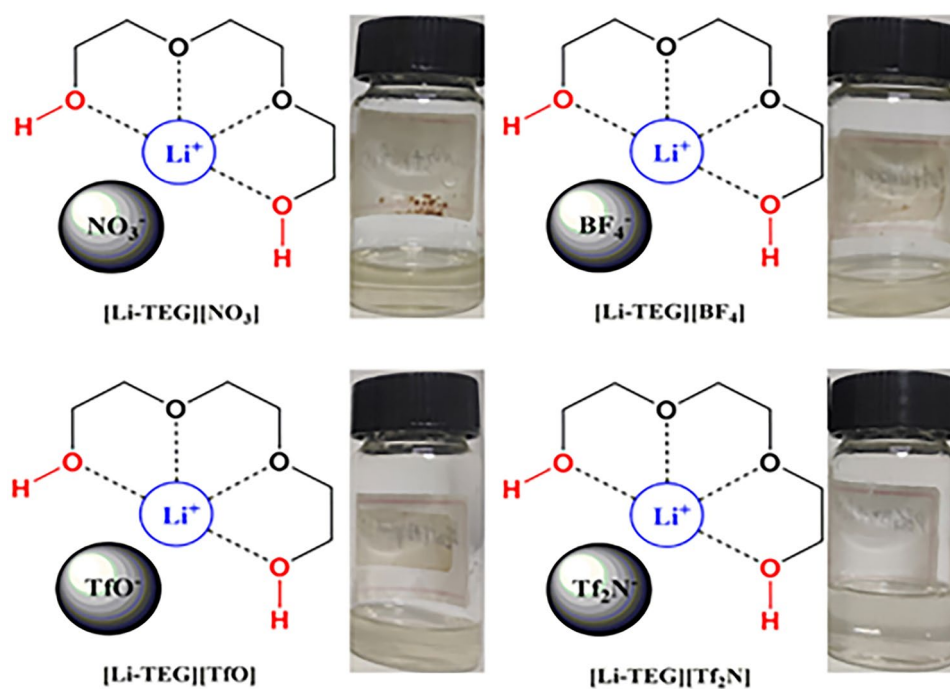


Fig. 5 Structures and pictures of Li-TEG-chelated ILs. Reproduced with permission from Ref. [51], Copyright 2022, John Wiley and Sons

this excellent performance was retained after ten absorption–desorption cycles. Additionally, the presence of CO_2 in melamine tail gases is unavoidable. Thus, the CO_2 absorption of optimized DESs was investigated. The results showed that the solubility of CO_2 was 0.91 mg g^{-1} , which is far lower than NH_3 solubility under the same conditions, showing great potential for the separation of NH_3 and CO_2 .

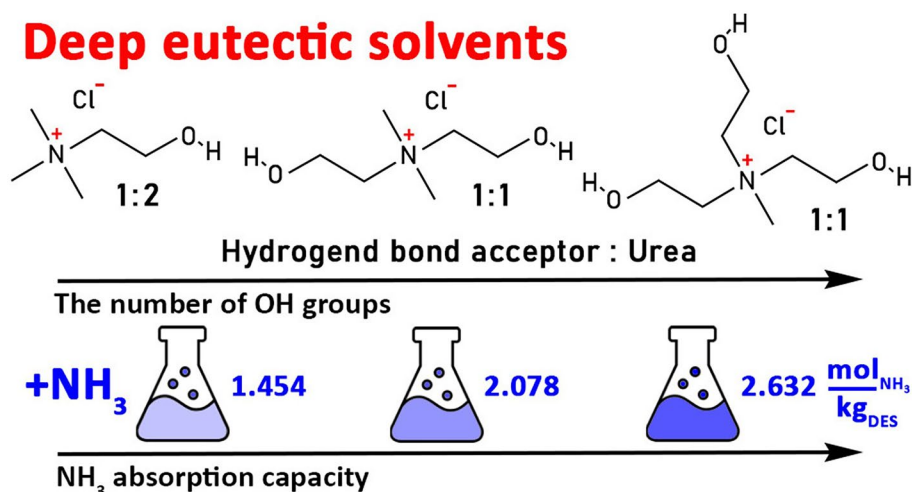
Subsequently, a series of DESs using ChCl as the HBA were developed for NH_3 capture owing to their excellent biodegradability and low price, including ChCl/Urea [54] and ChCl/dihydric alcohols [55]. Sun et al. [56] innovatively introduced metal chlorides, such as anhydrous MgCl_2 , NiCl_2 , MnCl_2 , and ZnCl_2 , into a binary Res/EG system to prepare ternary DESs, and the NH_3 capacity notably increased owing to the cooperating hydrogen bonding and Lewis acid–base interactions. In particular, the NH_3 absorption capacity of $\text{MgCl}_2/\text{Res}/\text{EG}$ (0.1:1:2) was 289 mg g^{-1} at 293 K and 100 kPa. In addition, the introduction of hydroxyl, amide, and carboxyl groups into the structure of HBDs in DESs was an effective method to obtain NH_3 absorbents with excellent performance [57–59]. ChCl-based DESs containing hydroxyl groups on HBDs exhibited higher NH_3 absorption capacity than DESs containing amide groups. The

optimal NH_3 capacity of ChCl/EG (1:2) reached 46 mg g^{-1} at 303.15 K and 546.1 kPa. Moreover, NH_3 absorption in this system was thermodynamically spontaneous according to thermodynamic property calculations, including standard Gibbs energy, dissolution enthalpy, and dissolution entropy [60]. Huang et al. [61, 62] further proposed introducing an HBD component with weak acidity into a ChCl-based system, which not only improved the NH_3 absorption capacity but also resulted in the reversible absorption of NH_3 .

Considering the potential risk that toxic components in DESs pose to human health and the environment, Li et al. [63] proposed “natural DESs” composed of ChCl and sugar. These DESs exhibited higher NH_3 capacities at low pressure and increased temperature compared with other reported DESs, which is important for practical applications, especially for low-concentration NH_3 capture. Most studies have focused on the rational design of HBD structures in DESs to regulate the NH_3 absorption performance, whereas Kazarina et al. [64–66] considered the functional group modification of HBAs. The substitution of hydroxyl groups in ChCl, as shown in Fig. 6, remarkably decreased the toxicity and enhanced NH_3 solubility via hydrogen bond interactions. The NH_3 absorption capacity was enhanced by increasing the number of hydroxyl groups of

Table 2 NH₃ absorption capacity of representative DESs

DES	<i>T</i> (K)	<i>P</i> (kPa)	NH ₃ absorption capacity (mg NH ₃ /g DES)	References
ChCl/Res/Gly (1:3:5)	313	101	130	[53]
ChCl/urea (1:2)	298	95	38	[54]
ChCl/1,4-BD (1:4)	303	115.8	57	[55]
MgCl ₂ /Res/EG (0.1:1:2)	313	100	205	[56]
Tz/Gly (1:3)	303	101.3	179	[57]
[TMPDA][Cl] ₂ /PhOH(1:7)	298	93.1	156	[58]
[Emim][Cl]/Tetz (1:1)	313	10.0	79	[59]
ChCl/EG (1:2)	313	100.5	46	[60]
ChCl/PhOH/EG (1:5:4)	298	101.3	164	[61]
ChCl/TetrZ/EG (3:7:14)	313	104.9	169	[62]
ChCl/xylose (1.5:1)	343	101.3	66	[63]
[MeC ₃ ^{OH} N]Cl/EG (1:2)	313.2	101	73	[64]
[Me ₂ C ^{OH} ₂ C ^{OH} N]Cl/Urea (1:1)	313.2	101.3	35.3	[65]
EaCl/AA (1:1)	313	96.4	65	[67]
EaCl/Gly (1: 2)	298	106.7	164	[68]
EaCl/PhOH (1:7)	298	101.3	85	[69]
EaCl/Res (1: 1)	298	101.2	182	[70]
3,4-DHAB + EG (1:3)	298	100	199	[71]
[Bmim][MeSO ₃]/urea (1:2)	313	172.6	18	[72]
[Im][NO ₃]/EG (1:3)	303	100	211	[73]
MAA/tetrazole (2:1)	313	102.9	136	[74]
KSCN/Gly (2:3)	313	100	101	[75]
NH ₄ SCN/Gly(2:3)	303	100	223	[75]
GI/AT (1:2)	303	101	90	[76]

**Fig. 6** Structure of HBAs modified by hydroxyl groups on cation and NH₃ absorption performance. Reproduced with permission from Ref. [66]. Copyright 2022, American Chemical Society

the choline cation. The absorption capacities of $[\text{Me}_2\text{C}^{\text{OH}}_2\text{N}]\text{Cl}/\text{Urea}$ with two hydroxyl groups and $[\text{MeC}^{\text{OH}}_3\text{N}]\text{Cl}/\text{Urea}$ with three hydroxyl groups were 35.3 and 44.7 mg NH_3/g DES at 313.2 K and 101.3 kPa, respectively, which is approximately twice that of ChCl/urea (2:3) under the same conditions.

In addition to ChCl -based DESs, much less expensive ethylamine hydrochloride (EaCl)-based DESs have also been developed. Similarly, the EaCl -based DESs with different hydrogen-bond donating ability or Brønsted acidity such as EaCl/AA [67], EaCl/Gly [68], EaCl/PhOH [69], and EaCl/Res [70], were explored for NH_3 capture. The effects of EaCl/HBD molar ratio, temperature, and pressure were investigated systematically. An appropriate EaCl/HBD molar ratio is beneficial for obtaining DESs with low viscosity and high NH_3 absorption capacity. Decreased temperature and increased pressure contributed to enhanced NH_3 absorption capacity.

However, the above-mentioned Cl -containing DESs have potential corrosivity hazards toward equipment in the practical applications. Zheng et al. [71] further proposed non-chloride DESs with multiple weak acidic sites (one carboxylic group and two phenolic hydroxyl groups) by dihydroxybenzoic acid (DHBA) and EG for selective NH_3 absorption. The DHAB/EGs DESs provided multiple hydrogen bond sites with NH_3 molecules, enabling exceptional and reversible NH_3 absorption with the value of 199 mg g^{-1} at 100 kPa and 298.15 K. Additionally, imidazole-based ILs without chloride elements were prepared as DESs, such as $[\text{Bmim}][\text{MeSO}_3]/\text{urea}$ [72], and $[\text{Im}][\text{NO}_3]/\text{EG}$ [73]; protic imidazole IL-based $[\text{Im}][\text{NO}_3]/\text{EG}$ DES with a molar ratio of 1:3 exhibited the highest capacity of 211 mg NH_3/g DES at 303 K and 100 kPa and great NH_3/CO_2 selectivity of 139.6 along with good recyclability. In addition, non-ILs binary DES systems have been developed for NH_3 absorption, such as N -methylacetamide(MAA)/tetrazole [74], $\text{NH}_4\text{SCN}/\text{Gly}$ [75], and GI/AT [76], in which the optimal NH_3 mass absorption capacity of $\text{NH}_4\text{SCN}/\text{Gly}$ (2:3) was as high as 223 mg/g DES at 303 K and 100 kPa because of the cooperative hydrogen bond interactions between NH_4^+ , OH , and NH_3 molecules.

4 Porous Solids for NH_3 Adsorption

Compared with liquid absorption materials, porous solids for NH_3 adsorption have been extensively studied [17, 77]. The abundant pores in solid materials provide the space for fast NH_3 transport, which also avoids the problems of corrosion

and low mass transfer efficiency resulting from acid scrubbing and the high viscosity of ILs. The reported porous solids can be roughly divided into four types: CIPMs, POPs, CPMs, and composite adsorbents, as shown in Fig. 7. Generally, CIPMs, such as activated carbon (AC), are low-cost and easy to fabricate, but the interaction between these materials and NH_3 molecules is weak. As a potential solution, POPs have been exploited, by the disordered pores formed by polymer segments/ordered pores and acidic groups enhance the NH_3 adsorption capacity. In addition, CPMs, such as MOFs, hydrogen-bonded organic frameworks (HOFs), and covalent organic frameworks (COFs, also belonging to POPs), usually exhibit high NH_3 adsorption capacities and fast adsorption kinetics owing to their ordered pore structures and strong interactions with NH_3 . Furthermore, composite adsorbents, especially IL-based composites, which couple the high NH_3 affinity of task-specific ILs with the porous properties of solid supports, are employed for NH_3 capture. In this section, we focus on the novel adsorbents reported in the last 5 years, covering the design ideas of the corresponding materials, NH_3 adsorption performance, and adsorption mechanism.

4.1 Conventional Inorganic Porous Materials

Conventional inorganic porous materials (CIPMs), including activated carbons (ACs) [78–80], zeolite [77], metal halides [81], and mesoporous silica/alumina [82], have been widely used for NH_3 capture because of their favorable characteristics, such as diverse pore architectures, high stability, and low cost. However, the NH_3 adsorption capacity of these materials is relatively low owing to their limited affinity toward NH_3 molecules. Therefore, the modification of functional groups to these CIPMs has been proposed to improve the NH_3 adsorption capacity. For instance, Zheng et al. [83] developed fiber-form AC modified by acidic oxygen groups, which exhibited a high NH_3 adsorption capacity of 50 mg g^{-1} . Li et al. [84] found that AC modified by HNO_3 exhibited the best NH_3 removal performance among three inorganic acid-modified ACs, with a maximum NH_3 adsorption amount of 40 mg g^{-1} , owing to the reduced adsorption energy caused by the co-adsorption of NH_3 with residual HNO_3 via a hydrogen bond network. More recently, Zhang et al. [85] demonstrated that ordered MS functionalized with a sulfonic group ($\text{OMS-SO}_3\text{H}$) exhibited ultra-high precision for NH_3 reversible adsorption and separation, benefiting

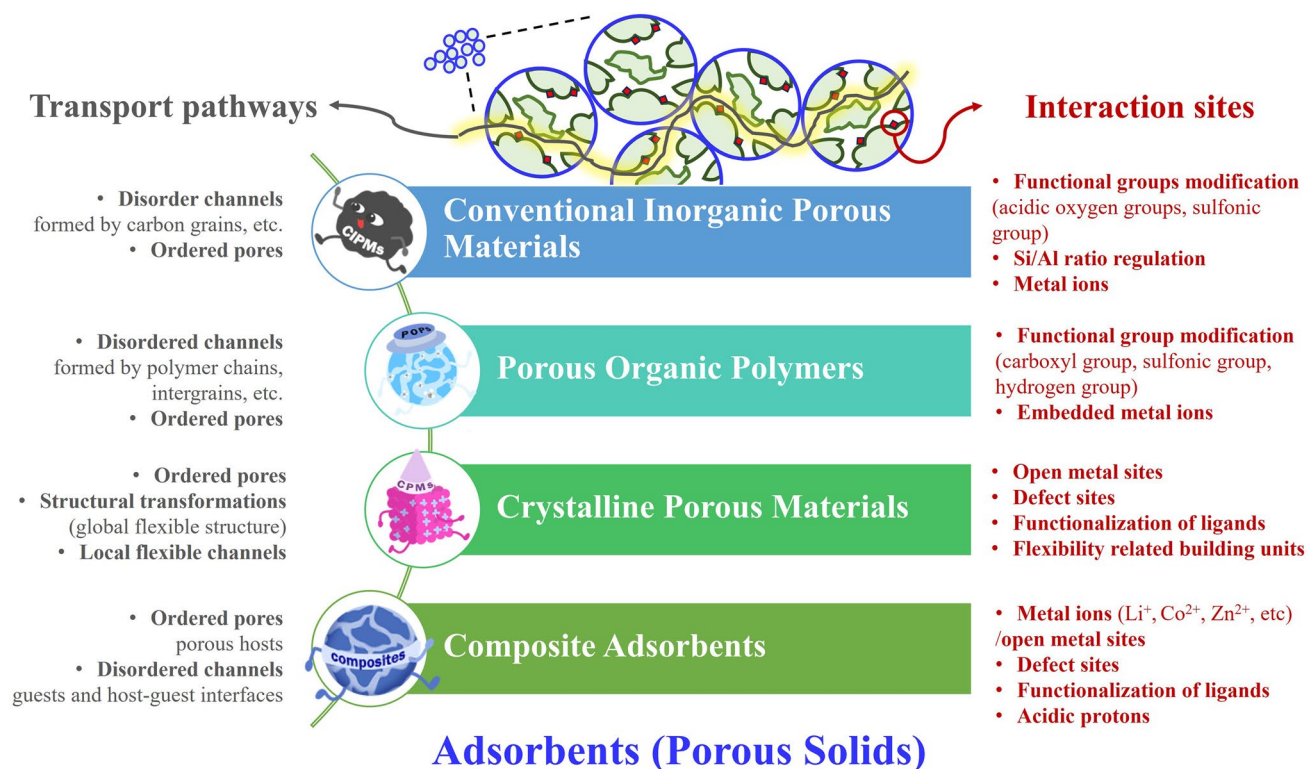


Fig. 7 Interaction sites and transport ways of four types of porous solids

from the high density of $-\text{SO}_3\text{H}$ superic acid sites in ordered mesochannels.

Zeolites are another popular material for NH_3 adsorption, and its properties, including acidity/basicity and hydrophilicity/hydrophobicity, can be tuned by varying the Si/Al ratio. Therefore, through interaction between NH_3 and zeolites, NH_3 adsorption performance can be finely regulated. Martos et al. [86] revealed that hydrogen bonds play an important role in NH_3 capture with pure or high-silica zeolites, as confirmed by experimental and molecular simulations. Ouyang et al. [87] further indicated that NH_3 adsorption capacity was inversely proportional to the Si/Al ratio. Exchanging the counter cation from Na^+ to Li^+ led to a higher NH_3 adsorption capacity owing to stronger interactions between Li^+ and NH_3 . In addition, the Al distribution in the nanopores and synthetic materials also affected the NH_3 adsorption performance [88, 89].

Metal halides can effectively capture NH_3 molecules by forming metal–ammonia complexes; however, regeneration at low temperatures is difficult [81]. Recently, Shen et al. [90] further studied the effect of metal halide types with the same metal cation and number of cycles on NH_3 adsorption

capacity. The NH_3 adsorption capacity followed the order $\text{CuCl}_2 > \text{CuBr}_2 > \text{CuI}$, and these materials underwent severe sintering during the high-temperature regeneration process, causing difficulty in recycling. Cao et al. [91] exploited a novel porous SrCl_2 structure with 96 wt% loading scaffolded by reduced graphene oxide networks to avoid sintering, which showed superior NH_3 adsorption capacity (50.5 mmol g^{-1}) and rapid absorption–desorption kinetics and maintained a porous structure accommodating the volume without disintegration during cycling experiments.

4.2 Porous Organic Polymers

Porous organic polymers (POPs) are among the most widely studied materials for gas separation owing to their various monomer geometries and excellent thermal/chemical stabilities derived from the covalent nature of polymers [92, 93]. The functionalization of POPs with tunable and strong acid sites is an effective way to improve NH_3 adsorption performance. In 2014, Van Humbeck et al. [94] firstly presented a series of diamondoid POPs densely functionalized with

carboxylic acids for NH_3 capture. Among various polymers, BPP-5 with a multiply interpenetrated structure dominated by pores smaller than 6 Å pores exhibits an NH_3 uptake of 17.7 mmol g^{-1} at 1 bar, and BPP-7 with larger pore size shows improved NH_3 absorption kinetics at low pressure (3.15 mmol g^{-1} at 480 ppm), but the recyclability of these POPs is not clear. Since then, various POPs modified by acid groups have been developed for NH_3 adsorption, such as COOH-copolymer PDAB-AA [95], PIM-1-COOH [96], H_3PO_4 modified POPs [97], H_2SO_4 -modified ethylene glycol dimethacrylate (EGDMA) polymers [98, 99] and sulfonated POPs [100], and the regeneration abilities of most materials have also been investigated systematically. Table 3 presents the NH_3 adsorption performance and regeneration properties of representative POPs.

Recently, Kan et al. [101] further reported a sulfonated and ordered mesoporous polymer (SOMP). The strong affinity of the $-\text{HSO}_3$ group with NH_3 in sequential pore space of SOMP, as shown in Fig. 8, not only enhances the molecular recognition ability but also facilitates NH_3 fast diffusion inside SOMP so that favorable NH_3 adsorption capacity (15.09 mmol g^{-1} at 25 °C and 1 bar) and excellent reversibility could be achieved. Additionally, a multi-step post-modification strategy was proposed to further improve the NH_3 adsorption performance of POPs. Kang et al. [102] found that a high NH_3 adsorption capacity, especially at low pressures, and excellent recyclability were obtained owing to the formation of high-density acidic functional groups ($-\text{COOH}$ and $-\text{HSO}_3$) induced by post-oxidation and post-sulfonation processes on poly(dimethylsiloxane) (PDMS)-coated hyper-crosslinked POPs. Furthermore, sequential post-sulfonation and post-alkylation reactions were developed to modify POPs for NH_3 capture. A record-high NH_3 capacity (4.03 mmol g^{-1}) at 500 ppm was achieved, and it adsorbed 0.48 mmol g^{-1} even at a concentration of 800 ppb. Simultaneously, the hydrophobic nature of alkyl chains offers rapid desorption kinetics and exceptional recyclability under dry and humid conditions at room temperature [103].

In addition to their ability to interact with acidic groups, the hydrogen bond-forming properties of NH_3 molecules are highly attractive for POPs. Lima et al. [104] demonstrated that hydrogen bonds play an important role in the NH_3 uptake by poly(amic acid) (PAA) by combining TGA with neutron spectroscopy, supported by DFT calculations. Besides, the hydrogen bond sites with $-\text{COOH}$ groups efficiently improved NH_3 adsorption performance of PAA, but

strong interaction also made complete regeneration difficult [105].

The incorporation of open metal sites and ionic units to prepare porous ionic polymers as NH_3 adsorbents is also promising. As shown in Fig. 9, Luo et al. [106] reported porous cobaltous thiocyanate ($\text{Co(II)(SCN)}_4^{2-}$, TA)-functionalized polyILs with an NH_3 uptake capacity of 12.2–20.1 mmol g^{-1} owing to cooperative interactions containing NH_3 coordinating with Co(II) instead of SCN^- and hydrogen bonding of H at the C2 atom in the imidazolium ring ($\text{C2H}\cdots\text{NH}_3$). At the same time, the competitive interaction between NH_3 and free SCN^- promoted NH_3 release, contributing to the good recyclability of the adsorbents. Moreover, the coordinative numbers of metal centers in polyILs with NH_3 molecules have a significant effect on the NH_3 capacity. For instance, high NH_3 adsorption capacity was achieved when the coordination number increased from $n=4$ ($\text{M}=\text{Cu/Zn}$) to $n=6$ ($\text{M}=\text{Co}$). Increasing the moderate size of the cross-linking agent R enhances the NH_3 capacity of PILs; however, oversizing R also reduces the porosity of polyILs [107]. Similarly, PIPs have also been explored, and multiple active sites containing charged skeletons, Lewis acid defects, and metal ions in Cu@PIP jointly promoted improved NH_3 adsorption performance and outstanding recyclability without structural collapse [93].

4.3 Crystalline Porous Materials

MOFs, which are typical CPMs, are one of the most promising candidates for NH_3 adsorption because their sorption selectivity is directly tunable as a function of the topology and chemical composition of the pores [19, 108–112]. Takahashi et al. [113] firstly demonstrated the possibility of historical pigment of Prussian blue and its analogs (CoHCC and CuHCF) for NH_3 capture. The NH_3 uptake capacity of Prussian blue is up to 12.5 mmol g^{-1} at 0.1 MPa owing to the NH_3 transformation into NH_4^+ with H_2O in air, which is much higher than that of standard NH_3 adsorbents (5.08–11.3 mmol g^{-1}). Subsequently, various MOFs for efficient NH_3 adsorption have been developed, in which the incorporation of open metal sites, functional sites on the ligand, and defect sites are effective measures to improve NH_3 adsorption performance. The NH_3 adsorption performance and regeneration properties of representative MOFs are listed in Table 4.

Table 3 NH₃ adsorption capacity and regeneration properties of representative POPs

Porous organic polymers	Functional groups	NH ₃ adsorption capacity	Regeneration conditions	Adsorption loss	References
BPP-5	–COOH	17.7 mmol g ^{–1} at 1 bar	NA ^a		[94]
BPP-7		3.15 mmol g ^{–1} at 480 ppm			
PDVB-2.0AA	–COOH	3.53 mmol g ^{–1} at 25 °C and 0.05 bar	80 °C, vacuum	11.2% (10 cycles)	[95]
PIM-1-COOH	–COOH	12.2 mmol g ^{–1} at 1 bar and 25 °C	RT and vacuum	~ 11.5% (3 cycles)	[96]
P2-CO2H	–COOH	16.1 mmol g ^{–1} at 1 bar and 25 °C 3.15 mmol g ^{–1} at 0.5 mbar and 25 °C	NA ^a		[98]
1-H ₂ SO ₄ -EGDMA	–COOH –SO ₃ H –OH	5.06 mmol g ^{–1} at 556 ppm and 20 °C	H ₂ SO ₄ washing, vacuum 80 °C	No loss (4 cycles)	[99]
MPOP-1.0-SO ₃ H	–SO ₃ H	10.96 mmol g ^{–1} at 1 bar and 25 °C	Ar flow, 160 °C	No loss (4 cycles)	[100]
SOMPs	–HSO ₃	15.09 mmol g ^{–1} at 25 °C and 1 bar 6.16 mmol g ^{–1} at 25 °C and 0.05 bar	0.001 bar, 150 °C	1.6% loss (30 cycles)	[101]
ITCS	–COOH	2.94 mmol g ^{–1} under humid conditions	NA ^a	No loss (10 cycles)	[102]
ITCS@PDMSX	–HSO ₃	2.1 mmol g ^{–1} under humid conditions		No loss (4 cycles)	
IS	–HSO ₃	4.03 mmol g ^{–1} at 500 ppm	NA ^a		[103]
IESC9	–OH	0.74 mmol g ^{–1} at 80% RH	He sweep	No loss (5 cycles)	
PAA	–COOH	10.7 mmol g ^{–1} at 25 °C and 1 bar	80 °C, 4 h	35% loss (1 cycle)	[105]
	–NH–	1.6 mmol g ^{–1} at 25 °C and 1 mbar			
Ph2Im-TBB-TA	Co(SCN) ₄ ^{2–}	20.1 mmol g ^{–1} at 25 °C and 1 bar	80 °C, vacuum	No loss (5 cycles)	[106]
	C2H in im ring	5.2 mmol g ^{–1} at 25 °C and 0.02 bar			
PVIm-R8-Co	Co ²⁺	20.1 mmol g ^{–1} at 25 °C and 1 bar	80 °C, vacuum	No loss (6 cycles)	[107]
Cu@PIP-X	Cu ²⁺	10.2 mmol g ^{–1} at 25 °C and 1 bar	100 °C, vacuum	No loss (5 cycles)	[93]
	B [–]				

^aNA is the abbreviation of not available

The incorporation of open metal sites in MOFs provides high NH₃ affinity, which is expected to remarkably improve NH₃ adsorption performance. For example, Dinca's group developed a series of triazole MOFs with open metal sites (Co, Ni, and Cu), in which Co₂Cl₂BBTA (BBTA = 1*H*,5*H*-benzo(1,2*d*), (4,5-*d'*)bistriazole) with smaller-pores exhibited greater capacities than their larger-pores BTDD-based counterparts (BTDD = bis(1*H*-1,2,3-triazolo[4,5-*b*],[4',5'-*i*])dibenzo[1,4]dioxin) benefiting from the higher density of

open metal sites. The static uptake is up to 19.79 mmol NH₃ g^{–1} at 1 bar and 298 K, which is more than twice the capacity of commercial activated carbon [114]. In contrast to the above-mentioned formation of NH₃-binding sites triggered by high-quality clusters, Carne-Sanchez et al. [115] reported metal–organic polyhedrals (MOPs) with Rh(II) as open metal sites for NH₃ capture. The low nuclear Rh(II) paddlewheel clusters in the synthesized MOFs firstly coordinated with NH₃ molecules, which further induced the

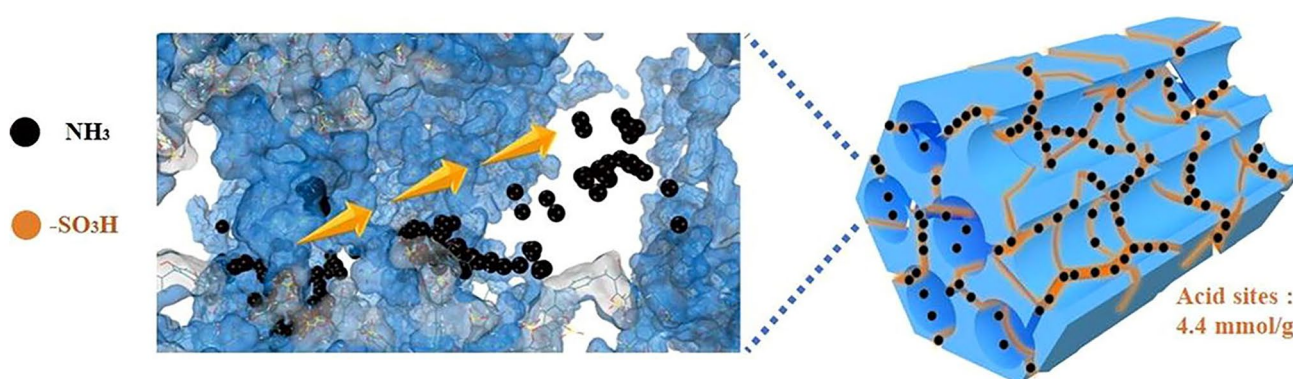


Fig. 8 NH_3 adsorption mechanism of SOMPs. Reproduced with permission from Ref. [101]. Copyright 2022, Elsevier

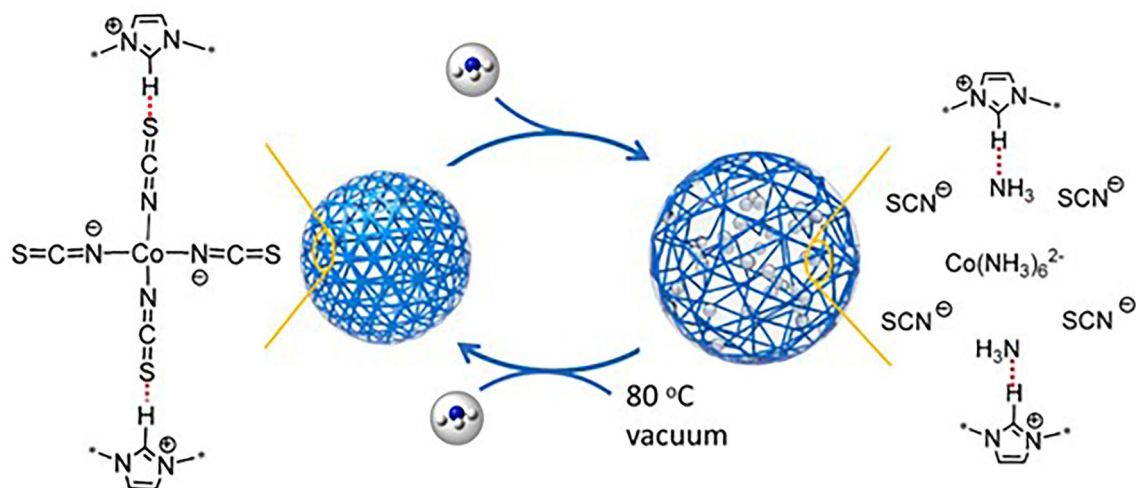


Fig. 9 Proposed mechanism of NH_3 adsorption with PIL-Tas. Reproduced with permission from Ref. [106]. Copyright 2021, Elsevier

adsorption of additional NH_3 molecules through H-bond interaction. This unique mechanism endows the prepared Rh-MOPs with a high NH_3 adsorption capacity exceeding 10 mmol g^{-1} , which can be easily regenerated via immersion in an acidic solution. The effect of open metal sites on NH_3 adsorption behavior was also investigated systematically. For example, CuBTC exhibited a higher ammonia uptake of $23.88 \text{ mmol g}^{-1}$ compared with others (ZnBTC, $11.33 \text{ mmol g}^{-1}$; FeBTC, 9.5 mmol g^{-1}) [116], and Al-PMOF showed greater NH_3 adsorption reversibility compared to those of isorecticular Ga-PMOF and In-PMOF [117]. Likewise, Zr_6 -NU-907 exhibited the highest NH_3 adsorption capacity at low pressure among the NU-907 family of MOFs, owing to the higher electronegativity of metal Zr ions. The in situ IR results further demonstrated that NH_4^+

and Lewis-bound NH_3 species were formed during NH_3 adsorption [118]. The $\text{Mg}_2(\text{dodpdc})$ exhibited record-high NH_3 capacity of $23.90 \text{ mmol g}^{-1}$ at 1 bar and 8.25 mmol g^{-1} at a low pressure of 0.57 mbar in a series of $\text{M}_2(\text{dodpdc})$ MOFs that were constructed from various divalent metal cations ($M = \text{Mg}^{2+}$, Mn^{2+} , Co^{2+} , Ni^{2+} , and Zn^{2+}) and a tetradentate ligand dobpdc^{4-} (Fig. 10a). At the same time, it was confirmed that $\text{Mg}_2(\text{dodpdc})$ shows excellent structural stability even for wet NH_3 owing to the higher affinity of Mg^{2+} for oxygen atoms than for nitrogen atoms, showing great potential for practical applications [119].

Functionalization of the ligand is another effective strategy for improving the NH_3 adsorption performance of MOFs. Nguyen et al. [120] functionalized ligands by incorporating electrophilic boron (B) centers, which

Table 4 NH₃ adsorption capacity and regeneration properties of representative CPMs

crystalline porous materials	T (°C)	P (bar)	NH ₃ adsorption capacity (mmol g ⁻¹)	Regeneration conditions	Adsorption loss	References
CoHCC	25	1	21.9	Vacuum, 150 °C	No loss (4 cycle)	[113]
Co ₂ Cl ₂ (BBTA)	25	1	17.95	Vacuum, 200 °C	~4% (3 cycle)	[114]
Rh-MOPs	25	1	12.9	Vacuum, 130 °C	52% (1 cycle)	[115]
CuBTC	25	1	23.88	Structural collapse		[116]
	25	BC ^a	8.8			[126]
Zr ₆ -NU-907	25	1	12.1	31.4% (3 successive cycles)		[118]
Al-PMOF	25	1	7.67	No loss (2 successive cycles)		[117]
Mg ₂ (dobpdc)	25	1	23.9	No loss (5 consecutive cycles)		[119]
	25	BC ^a	8.37			
SION105-Eu	30	1	5.7	70 °C for 30 min	No loss (5 cycles)	[120]
MFM-303(Al)	25	BC ^a	2.9	Vacuum, 80 °C	17% loss (29 cycles)	[121]
UiO-66-Cu ^{II}	0	1	16.9	Vacuum	No loss (15 cycles)	[125]
	25	BC ^a	4.15			
MFM-300(Al)	25	1	13.9	Dynamic vacuum < 1 h	No loss (50 cycles)	[129]
CAU-10-OH	25	BC ^a	3.5	Vacuum, 80 °C for 6 h	No loss (6 cycles)	[131]
Zn(NA) ₂	25	1	10.2	Vacuum, 150 °C for 70 min	No loss (3 cycles)	[134]
KUF-1 ^a	25	1	6.67	Vacuum, RT ^b	No loss (5 cycles)	[135]
[SrOOC]17-COF	10	1	19.8		44.8% loss (3 consecutive cycles)	[140]

^aBC is the abbreviation of breakthrough capacity

^bRT is the abbreviation of room temperature

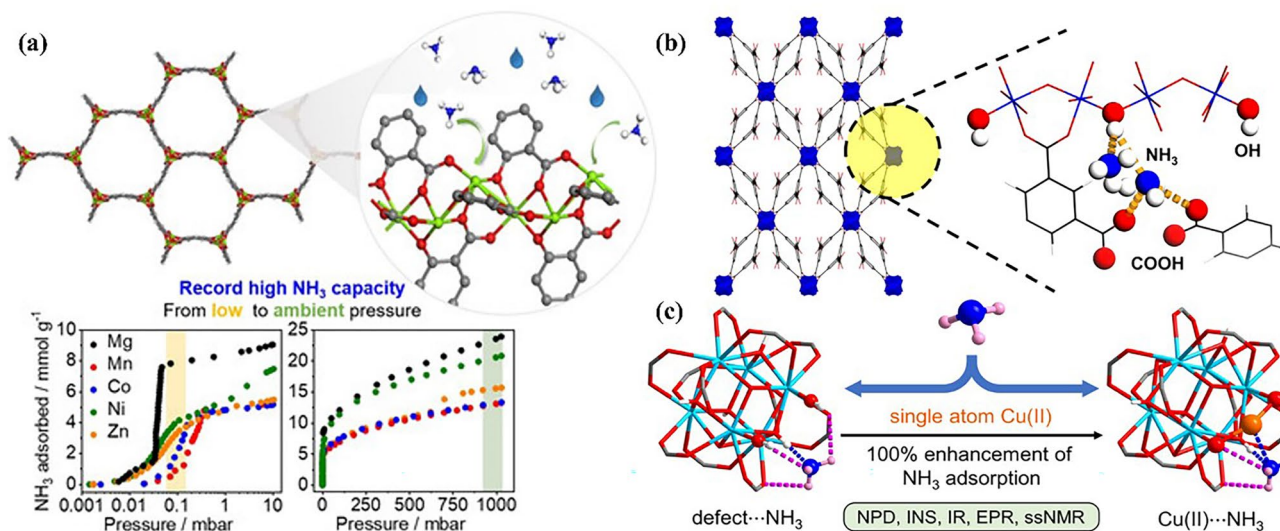


Fig. 10 **a** Atomic structure of M₂(dobpdc) (M²⁺=Mg²⁺, Mn²⁺, Co²⁺, Ni²⁺, and Zn²⁺) and NH₃ adsorption isotherms at 298 K. Reproduced with permission from Ref. [119]. Copyright 2020, John Wiley and Sons. **b** Structure of MFM-303(Al). Reproduced with permission from Ref. [121]. Copyright 2021, American Chemical Society. **c** Structure of UiO-66 material with defect site and Cu(II) Reproduced with permission from Ref. [125]. Copyright 2022, American Chemical Society

electrophilized the pores and promoted the capture of electrostatic NH₃ molecules. Moreover, the bulky duryl groups precluded strong acid–base B–N interactions to ensure the

robustness of MOFs in the presence of NH₃. Therefore, the prepared SION105-Eu MOF via this strategy is easily regenerated after NH₃ adsorption by simple heating at 75 °C. In

addition, a robust Al-based MOF, MFM-303(Al), functionalized with free carboxylic acid and hydroxyl groups, was developed for NH_3 capture, as shown in Fig. 10b [121]. Two carboxylate groups from each tetracarboxylic ligand molecule were bound to the Al(III) centers, whereas the other two remained uncoordinated and formed intramolecular hydrogen bonds with neighboring ligands. These acidic sites in the pores not only make MFM-303(Al) show excellent adsorption performance for low concentrations of NH_3 under both dry and wet conditions but also offer an exceptional packing density of NH_3 at 293 K (0.801 g cm^{-3}), comparable to that of solid NH_3 at 193 K (0.817 g cm^{-3}), which means that MFM-303(Al) could be used for NH_3 storage in practical applications.

Defective MOF construction by missing ligands or metal nodes can tune the nanostructure and pore size [122–124], thereby affecting the NH_3 adsorption performance. Ma et al. [125] simultaneously introduced defect sites and open Cu(I) and Cu(II) sites on a robust UiO-66 material, as shown in Fig. 10c, which exhibited high and reversible NH_3 adsorption capacity, avoiding the issues that MOFs with multiple coordination Cu(II) sites suffer from irreversible NH_3 sorption and structural degradation during adsorption. The excellent NH_3 adsorption–desorption reversibility of these MOFs predominantly resulted from the reversible change in the near-linear coordination geometry of the Cu(II) sites as a function of NH_3 binding.

Although MOFs possess high adsorption capacity and selectivity, most of them still face the challenge of structural degradation when in contact with NH_3 [126, 127]. Thus, enhancing the strength of the coordination bonds and tuning the moderate interaction between metal centers and NH_3 when designing MOFs should be emphatically considered. Yang et al. [128] designed a kind of ultra-stable MFM-300(Al), in which $\text{AlO}_4(\text{OH})_2$ was bridged by 3,3',5,5'-biphenyl-tetracarboxylic acid to form a “wine-rack” framework, which could store ammonia for at least 183 weeks without decreasing in the apparent domain size of changes in the unit cell volumes. The NH_3 adsorption capacity reached 15.7 mmol g^{-1} at 273 K and 1.0 bar, and there was no loss of NH_3 adsorption capacity over 50 cycles owing to the reversible H/D site exchange between the MOF and NH_3 molecules revealed by in situ neutron powder diffraction and synchrotron FTIR micro-spectroscopy [129]. Other isostructural analogs of MFM-300(M) (M = Fe, Cr, V) have also been reported, among which MFM-300(M)

(M = Cr, V^{III}) showed higher stability against humid NH_3 than MFM-300(M) (M = Fe, V^{IV}) [130]. Wang et al. [131] further synthesized super-stable CAU-10-based MOFs by choosing relatively inert Al^{3+} as metal nodes. Besides excellent long-term stability (more than 2 years), hydroxyl-functionalized CAU-10-O showed ultrahigh NH_3 adsorption capacity (3.5 mmol g^{-1} at $25.0 \text{ }^\circ\text{C}$) for low-concentration NH_3 (5000 ppm), high selectivity of NH_3 to N_2 (up to 4850), and mild regeneration conditions ($80 \text{ }^\circ\text{C}$ under vacuum for 6 h). Such great separation performance of CAU-10-OH was attributed to the multiple hydrogen bonding interactions ($\mu\text{-OH}\cdots\text{NH}_3$ and $-\text{OH}\cdots\text{NH}_3$) between NH_3 and CAU-10-OH.

Flexible MOFs with reversible structural transformations (topology, pore size or shape) usually exhibit a steep S-shaped adsorption curve, which can realize a high NH_3 working capacity and facile regeneration [132, 133]. For example, Chen et al. [134] found that the dehydration of $\text{M}(\text{NA})_2(\text{H}_2\text{O})_4$, (M = Zn, Co, Cu, Cd, NA = nicotinate) induces a structural transformation from zero-dimensional (0D) to two/three-dimensional (2D/3D), which is reversible after water adsorption. The layered 2D $\text{Zn}(\text{NA})_2$ exhibited a gate-opening effect at a pressure of 0.22 bar, leading to a two-step NH_3 uptake with a capacity of 10.2 mmol g^{-1} at 1 bar, while 2D $\text{Co}(\text{NA})_2$ showed a continually increasing NH_3 trend with an increase in pressure and an NH_3 adsorption capacity up to 17.5 mmol g^{-1} . For the transformed 3D $\text{Cu}(\text{NA})_2$ and $\text{Cd}(\text{NA})_2$, higher NH_3 adsorption rates and shorter adsorption equilibrium times were achieved after three cycles. Meanwhile, both MOFs showed great recyclability and could be regenerated under vacuum and heating conditions of $150 \text{ }^\circ\text{C}$ for 70 min. Similarly, Kang et al. [135] developed a novel sorbent called flexible HOFs KUF-1 for NH_3 adsorption, which showed unprecedented type IV adsorption behavior in the NH_3 isotherm at 298 K, with a capacity of 6.67 mmol g^{-1} at 1 bar (Fig. 11). This material can be completely regenerated at room temperature under vacuum. In addition, FDU-HOF-3 with self-healing properties and excellent capture performance at low NH_3 (8.13 mmol g^{-1} at 25 mbar) has also been developed [136]. Encouraged by reversible hydrogen network, Li et al. [137] further developed ionic frameworks $[\text{Ph}_3\text{ImH}][\text{NTf}_2]_2$ constructed from protic imidazolium ILs units through ionic and hydrogen bonding interactions for NH_3 capture, which presented selective NH_3 capture of $15.65 \text{ mmol g}^{-1}$ ($25 \text{ }^\circ\text{C}$ and 1 bar) and mild regeneration conditions ($80 \text{ }^\circ\text{C}$ and 1 mbar).

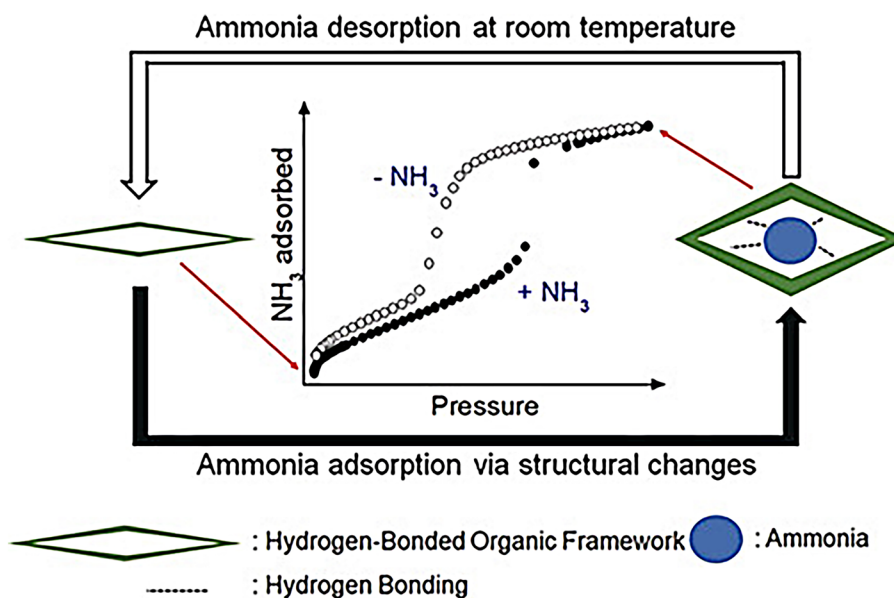


Fig. 11 Type IV NH_3 adsorption isotherm by HOF KUF-1a (Reproduced with permission from Ref. [135]. Copyright 2020, John Wiley and Sons)

Another emerging CPM, covalent organic frameworks (COFs), have also been explored for NH_3 adsorption. In contrast to MOFs, COFs are formed by connecting light atoms (hydrogen, boron, carbon, nitrogen, etc.) via strong covalent bonds. Thus, COFs usually exhibit higher NH_3 stability than MOFs based on the difference in bond strength. In addition, they have ordered pore structures that can effectively adsorb NH_3 molecules and be regulated according to the specific separation conditions [138, 139]. Inspired by the functional design of MOFs, decorating the pore walls of COFs with various open metal sites has also been proposed to improve NH_3 adsorption performance. For example, Yang et al. [140] adopted a surface pore engineering strategy to design multivariate COFs by decorating the pore walls with various functional units for NH_3 adsorption (Fig. 12). Owing to the high NH_3 affinity of synergistic multivariate and open metal sites, the COFs exhibited high NH_3 adsorption capacities (14.3 and 19.8 mmol g^{-1} at 298 and 283 K, respectively). Zhao et al. [141] investigated the NH_3 adsorption properties of COF-10 and its Li-doped derivatives using simulations. The NH_3 adsorption capacity could be improved by introducing more charged lithium atoms; however, this was not proportional to the number of lithium atoms. In addition, the charge distribution also affected the NH_3 adsorption behavior. In particular, a positive potential shield on the surface of

COF-10-6Li protected NH_3 from negative charge repulsion on the inner skeleton; thus, a remarkable enhancement in the NH_3 adsorption capacity was observed when six lithium atoms were introduced.

The actual performances of various materials under working conditions (containing H_2O and impurity molecules in handling gases) are important for practical applications. Although several MOFs have been explored, the number of MOFs reported for NH_3 capture from complex environments remains limited. Liu et al. [142] conducted a high-throughput computational screening (HTCS) of 2932 CoRe MOFs based on grand canonical Monte Carlo (GCMC) simulations to screen for the optimal MOF for NH_3 capture from humid gas. They found that the key to a high NH_3 capture performance was affinity or Henry's constant of MOFs toward NH_3 and water molecules. Previous research has indicated that NH_3 uptake by MOFs mostly exhibits a solubilization-like mechanism in the presence of H_2O molecules [143]. Hydrophobic MOFs possessed higher NH_3 selectivity, while hydrophilic MOFs exhibited higher NH_3 uptake despite strong adsorption competition from H_2O molecules. In addition, the presence of H_2O molecules could promote the enhancement of NH_3 uptake in the MOFs with a coefficient (describing the effect of H_2O adsorption on NH_3 uptake) of $\text{IC}_{\text{H}_2\text{O},\text{NH}_3} < 0$, but their ammonia uptake was still lower than that with $\text{IC}_{\text{H}_2\text{O},\text{NH}_3} > 0$, which is important for

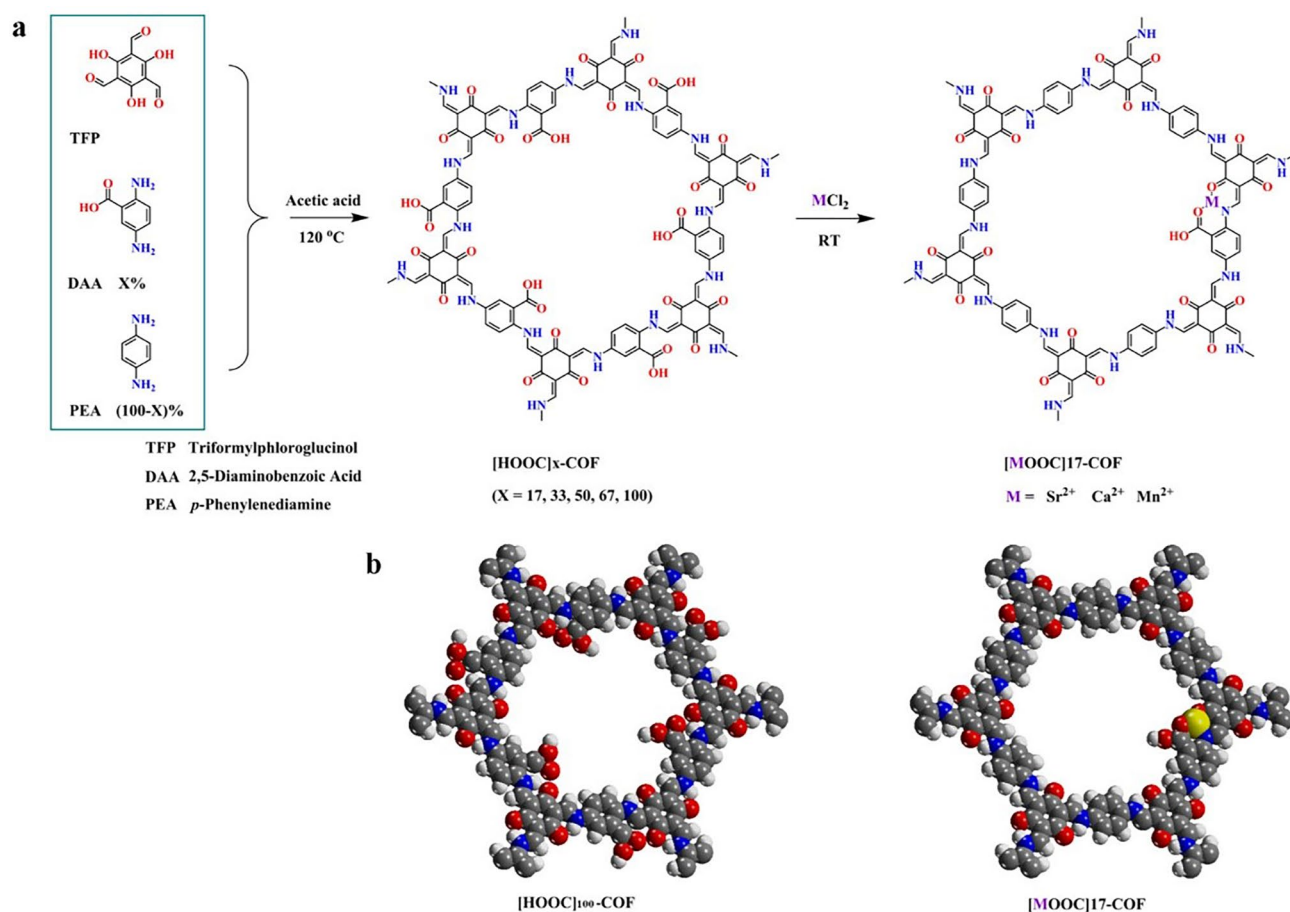


Fig. 12 **a** Scheme for surface pore engineering of COFs with various groups. **b** Possible pore structure of COFs with various groups (gray, C; blue, N; red, O; yellow, metal) (Reproduced with permission from Ref. [140]. Copyright 2018, American Chemical Society)

the structural design of MOFs. In fact, in NH_3 -containing gas from different NH_3 emission sources, not only are H_2O molecules present, but there are also other impurities such as SO_2 , which also greatly affect the NH_3 adsorption behaviors. Chen et al. [144] combined adsorption isotherms with DFT calculations to investigate this effect at low pressure. It was found that NH_3 is the most affinitive molecule to HKUST-1 among three molecules, while SO_2 was the most affinitive molecule to UIO-66; therefore, NH_3 is likely to displace pre-adsorbed SO_2 or H_2O on HKUST-1. Also, there is chemical adsorption on HKUST-1 and MIL-100(Fe) toward NH_3 , while NH_3 adsorption to UIO-66 likely involves physisorption.

4.4 Composite Adsorbents

Composite adsorbents combine the advantages of different materials in terms of NH_3 adsorption, such as metal

chloride/carbon cubes, metal chloride/COFs, and IL-based composites, showing good development prospects for NH_3 capture [145–148]. As a representative composite material, supported IL-phase (SILP) materials (Fig. 13a) have received more attention due to the cooperative effect of the porous support and functional ILs [48, 149, 150], which also solve the problems associated with the application of highly viscous or solid ILs for NH_3 separation. Functional ILs in SILP materials mainly provide high NH_3 affinity via interaction sites (see Sect. 3.1). Porous supports not only provide NH_3 transport pathways but also effectively disperse ILs to expose more accessible sites of ILs to further improve the NH_3 adsorption capacity.

Pioneering work on SILP for NH_3 adsorption was reported in 2014, where an AC support material was coated with $[\text{C}_2\text{ClIm}]\text{Cl}/\text{CuCl}_2$. The superior NH_3 adsorption capacity was predominantly attributed to strong interactions between

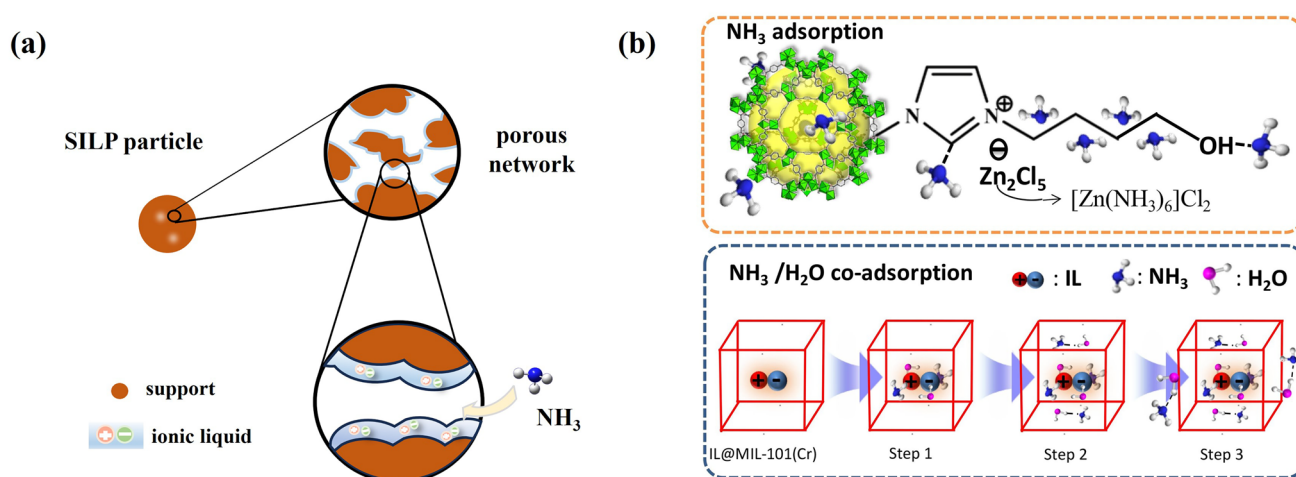


Fig. 13 **a** Schematic diagram of supported ILs phase materials. **b** Schematic diagram of mechanism of [BOHmim][Zn₂Cl₅]@MIL-101(Cr). Reproduced with permission from Ref. [156]. Copyright 2020, Elsevier

Cu²⁺ and NH₃ molecules [48]. However, regeneration was difficult under mild conditions. Therefore, subsequent studies have focused on the design of SILP materials for reversible NH₃ adsorption, in which the appropriate selection and matching of supports and ILs are of great importance. Yu et al. [151] selected protic ILs with reversible NH₃ adsorption to be supported on AC with low cost and large surface area for NH₃ adsorption. The results showed that 20 wt% [2-Mim][NTf₂]@AC-980 exhibited a higher NH₃ adsorption capacity of 68.61 mg g⁻¹ NH₃ at 303.15 K and 0.10 MPa (30% higher than that of pure AC) and excellent recyclability, benefiting from the synergistic interaction of hydrogen bonding between the ILs and NH₃ and hierarchical pores. To further improve the NH₃ adsorption performance, various task-specific ILs with multiple hydrogen-bond interaction sites/complexation sites and porous supports with different pore sizes were utilized to develop a variety of SILP materials, such as multiphoton ILs@HZSM-5 [152], hydroxyl ammonium protic ILs@MCM-41 [153], Zn-based ILs@FDU-12 [154], and MILs [Bmim]₂[Co(NCS)₄]@silica composites [155]. Enhanced NH₃ adsorption capacity and excellent adsorption–desorption performance were achieved in these materials, presenting great potential for application.

Encouraged by their tunable pore structure and chemical composition, MOFs have also been exploited as porous supports for constructing versatile SILPs. Han et al. [156] fabricated a highly stable IL@MOF composite material for NH₃ capture for the first time. [BOHmim][Zn₂Cl₅]@MIL-101(Cr) exhibited superior NH₃ uptake of 24.12 mmol g⁻¹

at 298 K and 1 bar, and such high NH₃ adsorption capacity could be maintained under humid NH₃ conditions. This excellent performance was related to the synergistic effect of multiple adsorption sites and the large free transport space provided by alkyl chains. Moreover, a small amount of adsorbed water provided additional NH₃ uptake, as shown in Fig. 11b. Subsequently, a [CAM][Cl]@MIL-101(Cr) composite was developed, and high-purity NH₃ was obtained in one step, as proven by a breakthrough experiment of an NH₃/CO₂ mixture showing superhigh NH₃/CO₂ separation factor of up to 1518 [157]. Shi et al. [158] anchored 43.4 wt% LiCl into the nanopores of MIL-53-(OH)₂ by charge transfer and hydrogen bonding for NH₃ capture. A record NH₃ adsorption capacity (33.9 mmol g⁻¹ at 1.0 bar and 25 °C) and superior selectivity of NH₃/N₂ (3571 at 25 °C), NH₃/CO₂ (30.3 at 80 °C) and NH₃/H₂O (15.6 at 50 °C) were achieved owing to synergistic action of NH₃ coordination with the highly dispersed Li⁺ in the MOF nanopores and hydrogen bonding of NH₃ with Cl⁻.

SILPs simultaneously improved the NH₃ adsorption capacity and promoted NH₃ transport, but the loading of ILs was always lower; therefore, the merits of liquid ILs were not fully displayed for the separation process [159–161]. A novel encapsulated ionic liquid (ENIL) was developed to achieve high IL loading and fully utilize the characteristics of ILs in confined spaces. Simultaneously, this material achieved the discretization of ILs from continuous to small drops, thereby increasing the surface contact area and improving the mass transfer rate. Palomar et al. [162, 163] prepared

an ENIL by confining [EtOHmim][BF₄] into hollow carbon submicron capsules. The unique core–shell structure as shown in Fig. 14 not only preserves the high NH₃ affinity and fluidity properties of ILs but also accelerates the absorption–desorption process compared with the continuous ILs phase. High IL content (> 85 wt%), nearly identical sorption capacity to pure ILs, and excellent regeneration properties were achieved in ENILs, providing a pioneering strategy for designing novel IL composites with ultrahigh IL loading for efficient NH₃ separation.

5 Porous Liquids for NH₃ Adsorption

Porous liquids (PLs) are attractive materials that combine the permanent porosity of porous solids with liquid fluidity so that they can be easily coupled with existing process equipment, such as pumps and pipelines. Different from traditional liquids consisting of only random, transient cavities between the liquid molecules (here called “extrinsic” porosity), PLs are made of porous hosts possessing persistent empty cavities (called “intrinsic” porosity), which are able to work as a gas transport pathway to provide rapid adsorption and high capacity. The concept of PLs was first proposed by James and coworkers [164] and can be divided into three types according to the existing way of the porous hosts as shown in Fig. 15 [165–167]. Type I is a neat liquid composed of fluid hosts with empty cavities, whereas Type II and Type III are essentially dissolved empty hosts or homogeneously dispersed framework materials in sterically hindered solvents, respectively. To date, the application of PLs has focused on gas capture and storage [167–170], while the synthesis of stable PLs remains a significant challenge

owing to intermolecular self-filling, collapse, or decomposition of the organic hosts and serious settling of solid particles.

The synthesis of fluid hosts with empty cavities is the key to obtaining Type I PLs. Giri et al. [171] grafted medium-length alkyl tails onto the surfaces of rigid organic iminospherand cages to synthesize PLs. Alkylation obviously reduced the melting point of the cage from > 300 °C to as low as 50 °C, making it possible to obtain fluid cages with empty cavities at relatively low temperatures. The liquida-tion of reported porous materials is also an effective method for preparing PLs (PLs prepared by this method are also called Type IV PLs, in which porosity is offered by non-discrete molecular species [172]). For example, Gaillac et al. [173] studied the melting process and liquid nature of porous ZIF-4 using in situ variable temperature XRD, ex situ neutron pair distribution function (PDF), and first-principles molecular dynamics (FPMD). They verified that the porosity of ZIF-4 was retained after melting process. In addition, hollow carbon or silica spheres grafted with ILs is another facile strategy for preparing a new PL phase. Zhang et al. [167] grafted positively charged organosilane onto the surface of hollow silica spheres, followed by an anion exchange reaction to prepare HS-liquid at room temperature, as shown in Fig. 16. TEM images, N₂-sorption isotherms, and small-angle X-ray scattering (SAXS) data revealed that well-defined hollow spheres were obtained. More importantly, the empty cavities significantly promoted CO₂/N₂ separation, showing attractive properties for target-specific applications, such as NH₃ separation.

In addition, the various MOFs and functional solvents used for NH₃ capture, as reported above, offer more

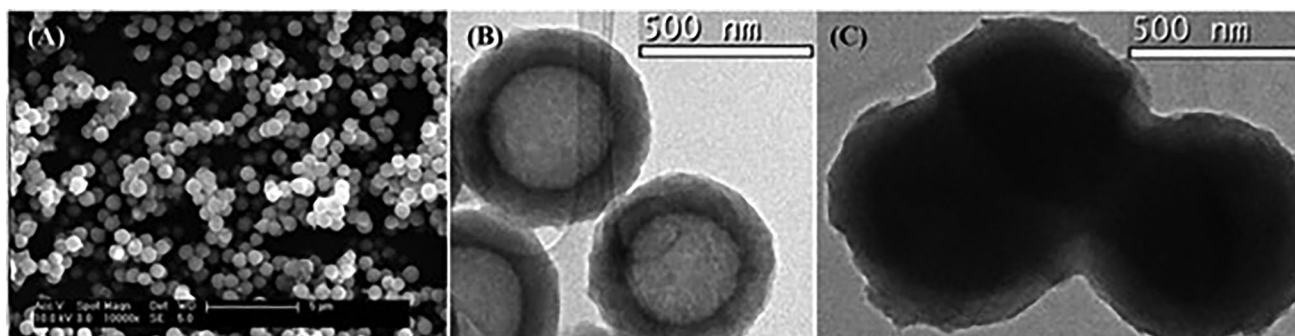


Fig. 14 a SEM image, b TEM images of hollow carbonaceous submicrocapsules. c TEM image of ENIL prepared with [EtOHmim][BF₄]. Reproduced with permission from Ref. [163], Copyright 2016, Royal Society of Chemistry

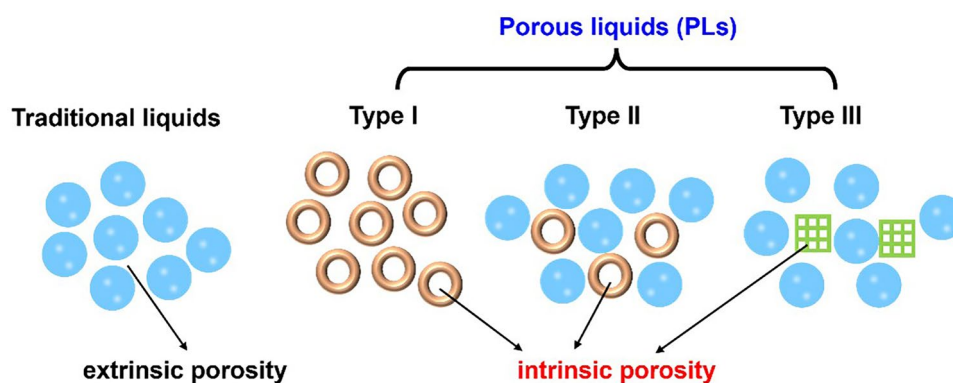


Fig. 15 Schematic diagram of traditional liquids and three different types of PLs. Adapted from Ref. [164]

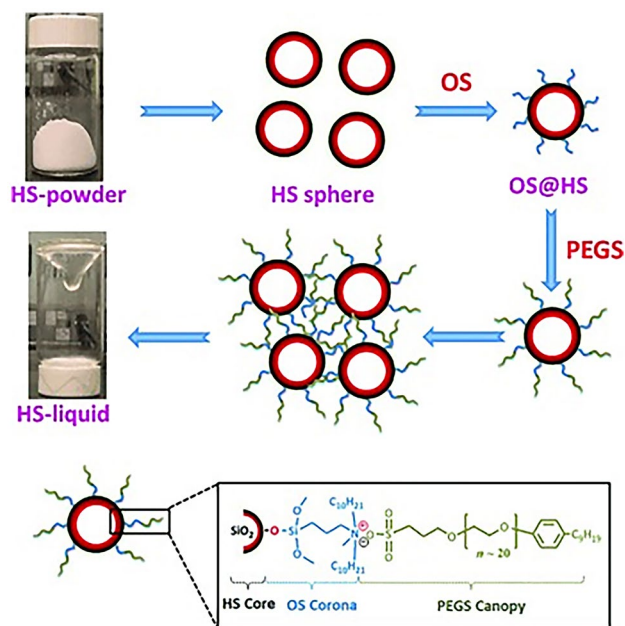


Fig. 16 Two-step synthetic strategy for porous liquid fabrication. HS, hollow silica, OS, organosilane. Reproduced with permission from Ref. [167]. Copyright 2014, John Wiley and Sons

opportunities for preparing Type-III PLs. The combination of MOFs with specific sterically hindered solvents, such as ILs, is expected to form new PLs with high gas uptake and separation performance. For example, Type-III PLs, including ZIF-8-[Bpy][NTf₂] [174] and ZIF-8-[DBU-PEG][NTf₂]₂ [168], were obtained by dispersing MOFs in ILs. Recently, Gomes et al. [27] also selected ZIF-8 and Mg-MOF-74 as porous hosts and dispersed them in [P₆₆₆₁₄][NTf₂], as shown in Fig. 17. The results showed that PLs were obtained by ZIF-8 but not by Mg-MOF-74 because of its small pore apertures (3.4 Å) preventing the penetration of large long-chain

cations. As a result, remarkable gas uptake performance (up to 150% more nitrogen and 100% more methane than pure IL) was realized at 303 K and 5 bar.

Overall, although examples of PLs for NH₃ ab-adsorption have not been reported, the development of PLs for NH₃ capture is attractive and promising from the perspective of fundamental research and practical applications. Importantly, the exciting results of CO₂ capture realized by PLs reveal their promising application in efficient NH₃ capture. At the same time, the aforementioned advanced ILs and various CPMs provide rich experience for designing novel PLs for NH₃ capture.

6 Emerging Membranes for NH₃ Separation

Membrane separation is another potential option for NH₃ capture because of its easy operation, low device occupancy, and energy saving [175–177]. Membrane separation can directly yield gaseous ammonia components without regeneration and has become increasingly attractive. However, unlike the extensive research on membranes for classical gases such as CO₂, studies on NH₃ capture using membranes are limited. Current research has primarily focused on the design of membrane materials to improve NH₃ permeability and selectivity. One effective measure is to introduce interaction sites to enhance NH₃ adsorption on the surfaces of membranes. Accelerating the NH₃ diffusivity in the membrane by constructing transport pathways is another effective strategy. Table 5 displays the NH₃ separation performances of representative membrane materials.

Polymeric membranes are the most typically reported NH₃ separation membranes because of their high

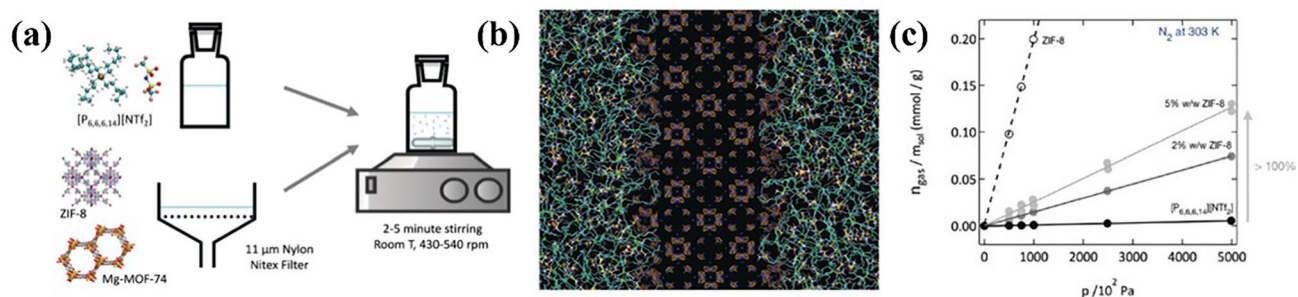


Fig. 17 **a** Preparation of the porous liquids. **b** Molecular simulation of the porous liquids show empty pores in ZIF-8. **c** Dissolution of N₂ in the PLs. Reproduced with permission from Ref. [27]. Copyright 2018, John Wiley and Sons

Table 5 NH₃ separation performance of membrane materials

Membrane Material	P_{NH_3} (Barrer)	α_{NH_3/N_2}	α_{NH_3/H_2}	Condition ^a	References
PDMS	6551.9	27.5		21 °C	[179]
TPX	188.4	25.5			
LDPE	15	25			
ETFE	17.3	34.6			
PTFE	0.5	1.3			
FEP	2.5	2.5			
Hyflon AD40	17.2	3.0			
Hyflon AD60	41	3.0			
Teflon AF1600	228.8	2.9			
Teflon AF2400	1635.4	3.0			
SBI-26 (CH-cast)	473	591		20 °C, 100 kPa	[182]
SBI-26 (THF-cast)	277	146			
POCE-PSS	612	50.6	50.1	25 °C, 100 kPa	[181]
Pebax 1657	595.8	406.7	70.1	RT ^b , 100 kPa	[184]
Nexar	496	566	88.6	RT ^b , 100 kPa	[186, 187]
POI-GI-POSS-0	489	157.7	104	25 °C, 110 kPa	[189]
POI-GI-POSS-0.1wt%	716	477.3	88.4		
POI-GI-POSS-0.5wt%	841	467.2	25.8		
POI-GI-POSS-1.0wt%	1032	543.2	21.3		
POI-GI-POSS-2.0wt%	434	4.6	10.3		
POI-GI-POSS-5.0wt%	528	5.2	9.9		
POI-GI-POSS-8.0wt%	210	1.7	1.8		
ZIF-21 ^c	25,910	35	12	RT ^b , ~ 141 kPa	[195]
MXene	18.4	24.6	14.53	100 kPa	[193]
PB/Au/AAO ^d	5.48	> 100	40	100 kPa	[194]
CA/PEG/MWCNTs-0	204	5		RT ^b , 300 kPa	[201]
CA/PEG/MWCNTs-5wt%	2127	70.9			
CA/PEG/MWCNTs-10wt%	2390	95.6			
CA/PEG/MWCNTs-15wt%	17,957	4.3			
CA/PEG/MWCNTs-20wt%	21,017	2.2			
CA/PEG/MWCNTs-30wt%	24,612	1.1			

^aTestig condition includes testing temperature and transmembrane pressure. ^bRT represents the room temperature. ^cThe thickness of separation layer is ~ 15 μm. ^dThe thickness of separation layer is 15–50 nm

processability, in which gas permeation basically obeys the solution-diffusion mechanism. The NH_3 transport properties of commercial cellulose acetate (CA) membranes were reported in 2006, and the results showed that the sorption process, dominated by hydrogen bond interactions between the NH_3 molecules and membranes, played an important role in NH_3 permeation [178]. Afterward, various polymers were exploited as membranes for NH_3 separation, such as fluorinated polymers [179, 180]. However, these polymeric membranes showed great permeability but little selectivity and still suffered a trade-off effect between permeability and selectivity (called the Robeson upper bound).

To overcome the above challenges, researchers have proposed the design of polymeric membranes with NH_3 -interacted sites, such as sulfonated copolymers, to enhance the selective adsorption and solubility coefficients of ammonia. Phillip et al. [181] regulated the domain size of sulfonated block copolymers and the degree of crosslinking to affect NH_3 separation performance. The results confirmed that the membrane designed using this strategy could retain high selectivity (mixed NH_3/N_2 selectivity > 90) compared to a Nafion membrane. Ansaloni et al. [182] further adjusted the membrane morphology of midblock-sulfonated pentablock ionomers (SBI-26 and SBI-52) by changing the type of casting solvent used to construct micro-domains conducive to NH_3 separation. Recently, fluorinated sulfonic acid polymer/ceramic composite membranes with high thermal stability were developed, in which the acidic sulfonic groups on the polymer chains acted as NH_3 sites, exhibiting NH_3 separation performance with NH_3 permeance of $> 2.31 \times 10^{-6}$

$\text{mol m}^{-2} \text{ s}^{-1} \text{ Pa}^{-1}$, NH_3/H_2 separation factor of 90, and NH_3/N_2 of 800 at 50 °C in a mixed system [183].

In addition, incorporating NH_3 -interacted small molecules, such as ILs, into the polymer matrix is expected to improve the NH_3 permeability and selectivity. As expected, the NH_3 permeability was remarkably enhanced with increasing IL content, benefiting from the enhanced NH_3 solubility [184, 185]. It is worth mentioning that the moderating interaction between membranes and NH_3 plays an important role in increasing NH_3 solubility, while excessively strong interactions also restrict NH_3 diffusivity. Therefore, the selection of appropriate ILs, such as hydroxyl task-specific ILs, is crucial for preparing membranes with high permeances. The optimum NH_3 permeability reached 3729.3 barrer with an NH_3/N_2 ideal selectivity of 1110.8, which are increases of 265.3% and 163.7%, respectively, compared to neat Pebax membrane. In addition, ILs enrich the ionic domains of block polymers to construct effective gas transport channels. The self-assembled NH_3 transport channels induced by ILs and high NH_3 affinity (Fig. 18) cooperatively promoted an increase in the NH_3 diffusion and solubility coefficients, resulting in superior NH_3 separation performance with an NH_3 permeability of 3565 barrer and NH_3/N_2 and NH_3/H_2 selectivity as high as 1865 and 364, respectively [186, 187].

Effective strategies include constructing a transport channel and increasing the free volume of the membrane to promote gas transport/diffusivity and enhance ammonia separation. Wang et al. [188] first adopted a simulation method to verify the NH_3 separation possibility of 2D-polyphthalocyanine (PPc) membranes with intrinsic pores. A high (H_2/N_2)/

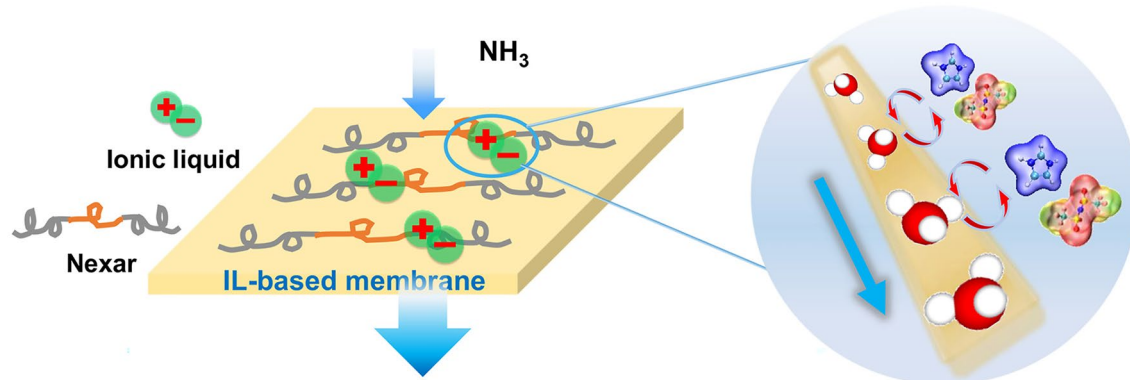


Fig. 18 Schematic diagram of IL/Nexar hybrid membranes for NH_3 separation (Reproduced with permission from Ref. [186]. Copyright 2021, Elsevier)

NH_3 selectivity of 10^7 was obtained at room temperature. Inspired by the above idea, Zaripov et al. [189] further prepared bulky agent octaglycidyl polyhedral oligomeric silsesquioxane (GI-POSS) branched membranes, in which the disordered nanopores formed by the polymer segments greatly promoted NH_3 transport. High ideal selectivity was achieved at GI-POSS contents of 0.5–1 wt%. Subsequently, various membrane materials such as porous silica [190], ceramics [191], and zeolites [192], and other inorganic membranes, have been developed to achieve selective separation with the help of different pore sizes. However, unsatisfactory separation performance has encouraged researchers to further develop novel membranes to meet application requirements. Strategies combining porous properties and preferential adsorption have been proposed. For example, Petukhov et al. [193] prepared a 2D MXene membrane for NH_3 separation in which acidic termination groups of interlayer galleries greatly promoted basic NH_3 adsorption, and the increase of interlayer distance caused by vapor adsorption within MXene's stacked structure also contributed to enhanced NH_3 diffusivity. Similarly, ultra-thin Prussian blue (PB) analog membranes with high NH_3 sorption capacity, pore channels (size of cavities < 0.3 nm), and high transformation ability of ammonia into NH_4^+ were prepared, achieving high NH_3 permeance exceeding $0.3 \text{ m}^3 \text{ (STP) m}^{-2} \text{ bar}^{-1} \text{ h}^{-1}$ and ultimate ideal NH_3/H_2 selectivity of 40 and NH_3/N_2 selectivity over 100 [194]. Furthermore, Wei et al. [195] coupled preferential adsorption and the sieving effect to prepare a ZIF-21 membrane with $\sim 2.8 \text{ \AA}$ polar channel. Polar pores with limited apertures could efficiently seize NH_3 molecules from gas mixtures. These two factors jointly promoted the ZIF-21 membrane to exhibit a high NH_3 permeance of 1727 GPU with NH_3/N_2 and NH_3/H_2 ideal selectivities of 35 and 12, respectively. Considering the similarity between NH_3 and H_2O in terms of polarity and molecular size, Yu et al. [196, 197] developed a Na^+ -gated nanochannel membrane via a secondary growth method, which allowed small and polar NH_3 molecules to permeate while blocking other non-polar and/or larger molecules, exhibiting remarkable selectivity ($\text{NH}_3/\text{H}_2 > 4280$ and $\text{NH}_3/\text{N}_2 > 10,000$ at $250 \text{ }^\circ\text{C}$ and 35 bar), excellent chemical stability, and long-term running stability.

Mixed matrix membranes (MMMs) have attracted increasing attention for NH_3 separation in recent years because of the synergistic effect of both polymer and porous components [198–200]. Raza et al. [201] introduced carboxylic group-functionalized multiwall carbon nanotubes

(COOH-MWCNTs) into a CA/PEG polymer matrix, which notably increased the permeability of NH_3 and N_2 owing to the enhanced voids and free volume. In addition, HKUST-1/PVDF MMMs were exploited by Cohen et al. [202] because HKUST-1 can bind with ammonia via Lewis acid–base interactions. Moreover, the HKUST-1 MMMs exhibited outstanding structural stability and maintained their ammonia capacity better than unstable powder under humid conditions. Our group [203] further combined HKUST-1 and protic IL [Bim][NTf₂] to improve NH_3 separation performance by employing hydrogen bond interactions. The optimal ternary MMM exhibited ideal NH_3/N_2 and NH_3/H_2 selectivities of 530.1 and 94.2, respectively. The optimal NH_3 permeability reached up to 3680.0 barrer, which is 260% and 129% higher than those of the pristine Pebax membrane and Pebax/HKUST-1 MMM, respectively.

7 Conclusions and Prospects

To effectively capture such hydrogen-rich, carbon-free, but highly corrosive molecules with triple the properties of energy, environment, and resources, great strides have been made in the development of advanced materials in the last decade. In this review, recent advances in NH_3 capture materials, particularly those over the past 5 years, were briefly summarized. Major obstacles for specific applications, such as absorbents (functional solvents), adsorbents (porous solids), and membranes, were identified based on extensive studies. The interaction sites and transport pathways play a crucial role in improving NH_3 capture performance. The potential application of the emerging hybrid technology, ab-adsorbents, using porous liquids as key capture materials, was also discussed. This review answers the question of how to connect advanced materials and NH_3 capture technology via modulation of interaction sites and transport pathways.

However, for these NH_3 capture technologies to be accepted as green strategies, the structure–property relationships between the materials and special parameters need to be further clarified, for which many challenges must be faced. In other words, there are worthwhile directions for researchers to further develop single/hybrid material designs and applications from either experimental or theoretical perspectives. The following aspects could be considered:

1. *Intelligent design & rational prediction* Designing novel materials and predicting their NH_3 capture performance

via a combination of theoretical calculations and experiments is highly desired. Various materials offer many possibilities for NH_3 capture; however, relying solely on experimental methods normally requires a long time. An effective strategy for obtaining an optimal solution is to utilize computational artificial intelligence (AI)-assisted molecular design and high-throughput screening technologies. Specifically, the properties of existing ammonia capture materials can be analyzed and important structures for efficient NH_3 capture can be extracted to build data- and mechanism-driven modes to further guide the development of high-performance materials. Furthermore, exploiting hybrid materials with complementary components, such as PLs, MOF@COF, and COF@MOFs, based on such recognition to further widen the variety of materials and obtain unforeseen structures has the potential to improve NH_3 capture performance. Interfacial properties, such as compatibility, interaction synergy, and growth mechanism, of hybrid materials are also worth exploring for further development of novel materials. In addition, the determination of the synthesis conditions and process parameters with the assistance of mobile robotic chemists is the most promising method for shortening the research and development process.

- Excellent performance & high stability* The development of NH_3 capture materials with high capacity, fast transport, and good stability remains challenging. Various functional materials have been developed based on the unique Lewis/Brønsted base and hydrogen bond formation properties of NH_3 molecules, while most of them still suffer from low capacity, slow kinetics, and structural collapse. In addition, although many NH_3 capture materials have been reported, breathing materials with a flexible nature (energy-saving synergistic adsorption–desorption) and dynamic properties (kinetic-induced non-equilibrium separation) are relatively limited. Therefore, the design of a robust system with both a high NH_3 capacity and soft porosity is a worthwhile direction to explore for practical applications.
- Scale-up* The large-scale preparation of materials should be considered to meet the requirements of industrial applications. Although significant progress has been achieved, especially in advanced materials for NH_3 capture, most current research is still limited to laboratories, and the yields of some materials are very small. Effective measures to boost scaled-up production and industrial applications need to be taken, such as screening inexpensive raw materials, simplifying synthesis steps, and using environmentally friendly synthetic methods. Specifically, expensive raw materials can be replaced with low-cost ones to synthesize various materials for NH_3 capture using a one-step rather than multi-step method to synthesize materials to omit complex purification process, using green solvents, such as water, as much as possible such as water to avoid volatile organic solvents. In addition, optimizing flow diagrams for chemical processes, heat exchange networks, and performing energetic–environmental–economic assessments using process simulation software are expected to improve energy efficiency and reduce operating costs to accelerate the process of industrialization. In future, AI-assisted reaction simulations will be a powerful platform for exploring effective solutions to overcome the drawbacks of stepwise amplification and accelerate industrialization.
- Practical evaluation* The practical utilization conditions of various materials should be considered. Most current studies have investigated capture performance under ambient pressure in pure gas. However, the composition, pressure, and NH_3 concentration of handling gases in real life are different, such as in the NH_3 synthesis process ($\text{NH}_3/\text{H}_2/\text{N}_2$, > 10 MPa, 10%–20% NH_3), personal protective equipment (NH_3/air , NH_3 < 5000 ppm), and NH_3 decomposition process (NH_3/H_2 , NH_3 < 0.1 ppm). Therefore, the data obtained in existing studies are far from reflecting realistic conditions. Based on the above analysis, it is necessary to upgrade existing equipment and perform operando characterizations to further evaluate the actual performance and reveal mechanisms in the future. Specifically, existing equipment must be improved to match the handling conditions (pressure and composition) of product gases to obtain a more realistic evaluation. The design of the internals should be optimized to meet fluid mechanics requirements, thereby achieving excellent mass and heat transfer in the equipment. Operando characterizations should be performed under practical working conditions to track the ab/adsorption and desorption of NH_3 molecules from various materials and to study possible structural changes under actual conditions to further reveal separation mechanisms [110, 204, 205].
- Integration process* Absorption–adsorption–membrane separation to develop an integrated technology to achieve self-adapting NH_3 capture is a promising direction for future research. Because massive amounts of NH_3 -containing gases from various sources face different separation requirements, multi-process integration is more efficient and applicable than a single technology. A rational process design for integrated technology is expected to achieve material cost and energy consumption savings.

Overall, functional solvents, porous solids, porous liquids, and membranes are potential alternatives for NH₃ capture. Although the road ahead is unknown, we firmly believe that various materials will become more competitive in the future through long-term and constant efforts.

Acknowledgements This work is financially supported by the National Natural Science Foundation of China (22178357), CAS Project for Young Scientists in Basic Research (YSBR-038), the Youth Innovation Promotion Association of the Chinese Academy of Sciences (2020047), the research fund of State Key Laboratory of Mesoscience and Engineering (MESO-23-A07, MESO-23-T02). Sincerely appreciate Prof. Suojiang Zhang (IPE, CAS) for his careful academic guidance and great support.

Declarations

Conflict of interest The authors declare no interest conflict. They have no known competing financial interest or personal relationships that could have appeared to influence the work reported in this paper. Ming-Shui Yao is an editorial board member for Nano-Micro Letters and was not involved in the editorial review or the decision to publish this article. All authors declare that there are no competing interests.

Open Access This article is licensed under a Creative Commons Attribution 4.0 International License, which permits use, sharing, adaptation, distribution and reproduction in any medium or format, as long as you give appropriate credit to the original author(s) and the source, provide a link to the Creative Commons licence, and indicate if changes were made. The images or other third party material in this article are included in the article's Creative Commons licence, unless indicated otherwise in a credit line to the material. If material is not included in the article's Creative Commons licence and your intended use is not permitted by statutory regulation or exceeds the permitted use, you will need to obtain permission directly from the copyright holder. To view a copy of this licence, visit <http://creativecommons.org/licenses/by/4.0/>.

References

- D. Feng, L. Zhou, T.J. White, A.K. Cheetham, T. Ma et al., Nanoengineering metal–organic frameworks and derivatives for electrosynthesis of ammonia. *Nano-Micro Lett.* **15**, 203 (2023). <https://doi.org/10.1007/s40820-023-01169-4>
- S. Zhang, Y. Zha, Y. Ye, K. Li, Y. Lin et al., Oxygen-coordinated single Mn sites for efficient electrocatalytic nitrate reduction to ammonia. *Nano-Micro Lett.* **16**, 9 (2023). <https://doi.org/10.1007/s40820-023-01217-z>
- Q. Hu, S. Qi, Q. Huo, Y. Zhao, J. Sun et al., Designing efficient nitrate reduction electrocatalysts by identifying and optimizing active sites of co-based spinels. *J. Am. Chem. Soc.* **146**, 2967–2976 (2024). <https://doi.org/10.1021/jacs.3c06904>
- F.B. Juangsa, A.R. Irhamna, M. Aziz, Production of ammonia as potential hydrogen carrier: review on thermochemical and electrochemical processes. *Int. J. Hydrog. Energy* **46**, 14455–14477 (2021). <https://doi.org/10.1016/j.ijhydene.2021.01.214>
- J. Li, S. Lai, D. Chen, R. Wu, N. Kobayashi et al., A review on combustion characteristics of ammonia as a carbon-free fuel. *Front. Energy Res.* **9**, 760356 (2021). <https://doi.org/10.3389/fenrg.2021.760356>
- X. Li, C. Deng, Y. Kong, Q. Huo, L. Mi et al., Unlocking the transition of electrochemical water oxidation mechanism induced by heteroatom doping. *Angew. Chem. Int. Ed.* **62**, 2309732 (2023). <https://doi.org/10.1002/anie.202309732>
- X. Li, H. Zhang, Q. Hu, W. Zhou, J. Shao et al., Amorphous NiFe oxide-based nanoreactors for efficient electrocatalytic water oxidation. *Angew. Chem. Int. Ed.* **62**, 2300478 (2023). <https://doi.org/10.1002/anie.202300478>
- Q. Hu, K. Gao, X. Wang, H. Zheng, J. Cao et al., Subnanometric Ru clusters with upshifted D band center improve performance for alkaline hydrogen evolution reaction. *Nat. Commun.* **13**, 3958 (2022). <https://doi.org/10.1038/s41467-022-31660-2>
- A.G. Bannov, M.V. Popov, A.E. Brester, P.B. Kurmashov, Recent advances in ammonia gas sensors based on carbon nanomaterials. *Micromachines* **12**, 186 (2021). <https://doi.org/10.3390/mi12020186>
- R.B. Bist, S. Subedi, L. Chai, X. Yang, Ammonia emissions, impacts, and mitigation strategies for poultry production: a critical review. *J. Environ. Manag.* **328**, 116919 (2023). <https://doi.org/10.1016/j.jenvman.2022.116919>
- K.E. Wyer, D.B. Kelleghan, V. Blanes-Vidal, G. Schaubberger, T.P. Curran, Ammonia emissions from agriculture and their contribution to fine particulate matter: a review of implications for human health. *J. Environ. Manag.* **323**, 116285 (2022). <https://doi.org/10.1016/j.jenvman.2022.116285>
- S.L. Nordahl, C.V. Preble, T.W. Kirchstetter, C.D. Scown, Greenhouse gas and air pollutant emissions from composting. *Environ. Sci. Technol.* **57**, 2235–2247 (2023). <https://doi.org/10.1021/acs.est.2c05846>
- J. Tian, B. Liu, Ammonia capture with ionic liquid systems: a review. *Crit. Rev. Environ. Sci. Technol.* **52**, 767–809 (2022). <https://doi.org/10.1080/10643389.2020.1835437>
- L. Zhang, H. Dong, S. Zeng, Z. Hu, S. Hussain et al., An overview of ammonia separation by ionic liquids. *Ind. Eng. Chem. Res.* **60**, 6908–6924 (2021). <https://doi.org/10.1021/acs.iecr.1c00780>
- S. Zeng, Y. Cao, P. Li, X. Liu, X. Zhang, Ionic liquid–based green processes for ammonia separation and recovery. *Curr. Opin. Green Sustain. Chem.* **25**, 100354 (2020). <https://doi.org/10.1016/j.cogsc.2020.100354>
- K. Vikrant, V. Kumar, K.-H. Kim, D. Kukkar, Metal–organic frameworks (MOFs): potential and challenges for capture and abatement of ammonia. *J. Mater. Chem. A* **5**, 22877–22896 (2017). <https://doi.org/10.1039/C7TA07847A>
- T. Islamoglu, Z. Chen, M.C. Wasson, C.T. Buru, K.O. Kirlikovali et al., Metal–organic frameworks against toxic chemicals. *Chem. Rev.* **120**, 8130–8160 (2020). <https://doi.org/10.1021/acs.chemrev.9b00828>



18. Y. Zhang, X. Cui, H. Xing, Recent advances in the capture and abatement of toxic gases and vapors by metal–organic frameworks. *Mater. Chem. Front.* **5**, 5970–6013 (2021). <https://doi.org/10.1039/d1qm00516b>
19. X. Han, S. Yang, M. Schröder, Metal–organic framework materials for production and distribution of ammonia. *J. Am. Chem. Soc.* **145**, 1998–2012 (2023). <https://doi.org/10.1021/jacs.2c06216>
20. X. Sun, G. Li, S. Zeng, L. Yuan, L. Bai et al., Ultra-high NH₃ absorption by triazole cation-functionalized ionic liquids through multiple hydrogen bonding. *Sep. Purif. Technol.* **307**, 122825 (2023). <https://doi.org/10.1016/j.seppur.2022.122825>
21. L. Yuan, X. Zhang, B. Ren, Y. Yang, Y. Bai et al., Dual-functionalized protic ionic liquids for efficient absorption of NH₃ through synergistically physicochemical interaction. *J. Chem. Technol. Biotechnol.* **95**, 1815–1824 (2020). <https://doi.org/10.1002/jctb.6381>
22. A.J. Rieth, Y. Tulchinsky, M. Dincă, High and reversible ammonia uptake in mesoporous azolate metal–organic frameworks with open Mn Co, and Ni sites. *J. Am. Chem. Soc.* **138**, 9401–9404 (2016). <https://doi.org/10.1021/jacs.6b05723>
23. Y. Su, K.-I. Otake, J.-J. Zheng, S. Horike, S. Kitagawa et al., Separating water isotopologues using diffusion-regulatory porous materials. *Nature* **611**, 289–294 (2022). <https://doi.org/10.1038/s41586-022-05310-y>
24. A. Bavykina, A. Cadiau, J. Gascon, Porous liquids based on porous cages, metal organic frameworks and metal organic polyhedra. *Coord. Chem. Rev.* **386**, 85–95 (2019). <https://doi.org/10.1016/j.ccr.2019.01.015>
25. Z. Zhang, B. Yang, B. Zhang, M. Cui, J. Tang et al., Type II porous ionic liquid based on metal–organic cages that enables L-tryptophan identification. *Nat. Commun.* **13**, 2353 (2022). <https://doi.org/10.1038/s41467-022-30092-2>
26. H. Liu, B. Liu, L.-C. Lin, G. Chen, Y. Wu et al., A hybrid absorption-adsorption method to efficiently capture carbon. *Nat. Commun.* **5**, 5147 (2014). <https://doi.org/10.1038/ncomms6147>
27. M. Costa Gomes, L. Pison, C. Červinka, A. Padua, Porous ionic liquids or liquid metal–organic frameworks? *Angew. Chem. Int. Ed.* **57**, 11909–11912 (2018). <https://doi.org/10.1002/anie.201805495>
28. Z. Wang, A. Ozcan, G.A. Craig, F. Haase, T. Aoyama et al., Pore-networked gels: permanently porous ionic liquid gels with linked metal–organic polyhedra networks. *J. Am. Chem. Soc.* **145**, 14456–14465 (2023). <https://doi.org/10.1021/jacs.3c03778>
29. H. Dong, X. Yuan, Y. Wang, Y. Lu, H. He, Preparation of two-dimensional nanoconfined ionic liquid membrane and its molecular mechanism of CO₂ separation. *Chem. Eng. Sci.* **283**, 119393 (2024). <https://doi.org/10.1016/j.ces.2023.119393>
30. B. Yang, H. Jiang, L. Bai, Y. Bai, T. Song et al., Application of ionic liquids in the mixed matrix membranes for CO₂ separation: an overview. *Int. J. Greenh. Gas Contr.* **121**, 103796 (2022). <https://doi.org/10.1016/j.ijggc.2022.103796>
31. X. Zhang, X. Zhang, H. Dong, Z. Zhao, S. Zhang et al., Carbon capture with ionic liquids: overview and progress. *Energy Environ. Sci.* **5**, 6668 (2012). <https://doi.org/10.1039/c2ee21152a>
32. A. Yokozeki, M.B. Shiflett, Vapor–liquid equilibria of ammonia+ionic liquid mixtures. *Appl. Energy* **84**, 1258–1273 (2007). <https://doi.org/10.1016/j.apenergy.2007.02.005>
33. W. Shi, E.J. Maginn, Molecular simulation of ammonia absorption in the ionic liquid 1-ethyl-3-methylimidazolium bis(trifluoromethylsulfonyl)imide ([emim][Tf₂N]). *AIChE. J.* **55**, 2414–2421 (2009). <https://doi.org/10.1002/aic.11910>
34. J. Palomar, M. Gonzalez-Miquel, J. Bedia, F. Rodriguez, J.J. Rodriguez, Task-specific ionic liquids for efficient ammonia absorption. *Sep. Purif. Technol.* **82**, 43–52 (2011). <https://doi.org/10.1016/j.seppur.2011.08.014>
35. J. Bedia, J. Palomar, M. Gonzalez-Miquel, F. Rodriguez, J.J. Rodriguez, Screening ionic liquids as suitable ammonia absorbents on the basis of thermodynamic and kinetic analysis. *Sep. Purif. Technol.* **95**, 188–195 (2012). <https://doi.org/10.1016/j.seppur.2012.05.006>
36. Z. Li, X. Zhang, H. Dong, X. Zhang, H. Gao et al., Efficient absorption of ammonia with hydroxyl-functionalized ionic liquids. *RSC Adv.* **5**, 81362–81370 (2015). <https://doi.org/10.1039/C5RA13730F>
37. M.S. Larrechi, A. Cera-Manjarres, D. Salavera, A. Coronas, Quantitative analysis of the interaction of ammonia with 1-(2-hydroxyethyl)-3-methylimidazolium tetrafluoroborate ionic liquid. Understanding the volumetric and transport properties of their mixtures. *J. Mol. Liq.* **301**, 112440 (2020). <https://doi.org/10.1016/j.molliq.2020.112440>
38. D. Shang, X. Zhang, S. Zeng, K. Jiang, H. Gao et al., Protic ionic liquid[Bim][NTf₂] with strong hydrogen bond donating ability for highly efficient ammonia absorption. *Green Chem.* **19**, 937–945 (2017). <https://doi.org/10.1039/c6gc03026b>
39. B. Yang, D. Shang, W. Tu, S. Zeng, L. Bai et al., Studies on the physical properties variations of protic ionic liquid during NH₃ absorption. *J. Mol. Liq.* **296**, 111791 (2019). <https://doi.org/10.1016/j.molliq.2019.111791>
40. T. Zhao, S. Zeng, Y. Li, Y. Bai, L. Bai et al., Molecular insight into the effect of ion structure and interface behavior on the ammonia absorption by ionic liquids. *AIChE. J.* **68**, e17860 (2022). <https://doi.org/10.1002/aic.17860>
41. D. Shang, S. Zeng, X. Zhang, X. Zhang, L. Bai et al., Highly efficient and reversible absorption of NH₃ by dual functionalised ionic liquids with protic and Lewis acidic sites. *J. Mol. Liq.* **312**, 113411 (2020). <https://doi.org/10.1016/j.molliq.2020.113411>
42. L. Yuan, H. Gao, H. Jiang, S. Zeng, T. Li et al., Experimental and thermodynamic analysis of NH₃ absorption in dual-functionalized pyridinium-based ionic liquids. *J. Mol. Liq.* **323**, 114601 (2021). <https://doi.org/10.1016/j.molliq.2020.114601>
43. X. Luo, R. Qiu, X. Chen, B. Pei, J. Lin et al., Reversible construction of ionic networks through cooperative hydrogen bonds for efficient ammonia absorption. *ACS Sustain.*

- Chem. Eng. **7**(11), 9888–9895 (2019). <https://doi.org/10.1021/acssuschemeng.9b00554>
44. R. Qiu, X. Luo, L. Yang, J. Li, X. Chen et al., Regulated threshold pressure of reversibly sigmoidal NH_3 absorption isotherm with ionic liquids. *ACS Sustain. Chem. Eng.* **8**, 1637–1643 (2020). <https://doi.org/10.1021/acssuschemeng.9b06555>
45. D. Deng, X. Deng, K. Li, H. Fang, Protic ionic liquid ethanolamine thiocyanate with multiple sites for highly efficient NH_3 uptake and NH_3/CO_2 separation. *Sep. Purif. Technol.* **276**, 119298 (2021). <https://doi.org/10.1016/j.seppur.2021.119298>
46. T. Makino, M. Kanakubo, NH_3 absorption in Brønsted acidic imidazolium- and ammonium-based ionic liquids. *New J. Chem.* **44**, 20665–20675 (2020). <https://doi.org/10.1039/d0nj04743k>
47. W. Chen, S. Liang, Y. Guo, X. Gui, D. Tang, Investigation on vapor–liquid equilibria for binary systems of metal ion-containing ionic liquid[bmim]Zn₂Cl₃/NH₃ by experiment and modified UNIFAC model. *Fluid Phase Equilib.* **360**, 1–6 (2013). <https://doi.org/10.1016/j.fluid.2013.09.011>
48. F.T.U. Kohler, S. Popp, H. Klefer, I. Eckle, C. Schrage et al., Supported ionic liquid phase (SILP) materials for removal of hazardous gas compounds—efficient and irreversible NH_3 adsorption. *Green Chem.* **16**, 3560–3568 (2014). <https://doi.org/10.1039/C3GC42275E>
49. S. Zeng, L. Liu, D. Shang, J. Feng, H. Dong et al., Efficient and reversible absorption of ammonia by cobalt ionic liquids through Lewis acid–base and cooperative hydrogen bond interactions. *Green Chem.* **20**, 2075–2083 (2018). <https://doi.org/10.1039/C8GC00215K>
50. J. Wang, S. Zeng, F. Huo, D. Shang, H. He et al., Metal chloride anion-based ionic liquids for efficient separation of NH_3 . *J. Clean. Prod.* **206**, 661–669 (2019). <https://doi.org/10.1016/j.jclepro.2018.09.192>
51. Z. Cai, J. Zhang, Y. Ma, W. Wu, Y. Cao et al., Chelation-activated multiple-site reversible chemical absorption of ammonia in ionic liquids. *AIChE. J.* **68**, e17632 (2022). <https://doi.org/10.1002/aic.17632>
52. L.L. Sze, S. Pandey, S. Ravula, S. Pandey, H. Zhao et al., Ternary deep eutectic solvents tasked for carbon dioxide capture. *ACS Sustain. Chem. Eng.* **2**, 2117–2123 (2014). <https://doi.org/10.1021/sc5001594>
53. Y. Li, M.C. Ali, Q. Yang, Z. Zhang, Z. Bao et al., Hybrid deep eutectic solvents with flexible hydrogen-bonded supramolecular networks for highly efficient uptake of NH_3 . *ChemSusChem* **10**, 3368–3377 (2017). <https://doi.org/10.1002/cssc.201701135>
54. F.-Y. Zhong, K. Huang, H.-L. Peng, Solubilities of ammonia in choline chloride plus urea at (298.2–353.2) K and (0–300) kPa. *J. Chem. Thermodyn.* **129**, 5–11 (2019). <https://doi.org/10.1016/j.jct.2018.09.020>
55. X. Deng, X. Duan, L. Gong, D. Deng, Ammonia solubility, density, and viscosity of choline chloride–dihydric alcohol deep eutectic solvents. *J. Chem. Eng. Data* **65**, 4845–4854 (2020). <https://doi.org/10.1021/acs.jced.0c00386>
56. X. Sun, Q. Wang, S. Wu, X. Zhao, L. Wei et al., Metal chlorides-promoted ammonia absorption of deep eutectic solvent. *Int. J. Hydrogen Energy* **47**(36), 16121–16131 (2022). <https://doi.org/10.1016/j.ijhydene.2022.03.101>
57. D. Deng, X. Duan, B. Gao, C. Zhang, X. Deng et al., Efficient and reversible absorption of NH_3 by functional azole–glycerol deep eutectic solvents. *New J. Chem.* **43**, 11636–11642 (2019). <https://doi.org/10.1039/C9NJ01788G>
58. Y. Cao, J. Zhang, Y. Ma, W. Wu, K. Huang et al., Designing low-viscosity deep eutectic solvents with multiple weak–acidic groups for ammonia separation. *ACS Sustain. Chem. Eng.* **9**, 7352–7360 (2021). <https://doi.org/10.1021/acssuschemeng.1c01674>
59. W.-J. Jiang, J.-B. Zhang, Y.-T. Zou, H.-L. Peng, K. Huang, Manufacturing acidities of hydrogen-bond donors in deep eutectic solvents for effective and reversible NH_3 capture. *ACS Sustain. Chem. Eng.* **8**, 13408–13417 (2020). <https://doi.org/10.1021/acssuschemeng.0c04215>
60. X. Duan, B. Gao, C. Zhang, D. Deng, Solubility and thermodynamic properties of NH_3 in choline chloride-based deep eutectic solvents. *J. Chem. Thermodyn.* **133**, 79–84 (2019). <https://doi.org/10.1016/j.jct.2019.01.031>
61. F.-Y. Zhong, H.-L. Peng, D.-J. Tao, P.-K. Wu, J.-P. Fan et al., Phenol-based ternary deep eutectic solvents for highly efficient and reversible absorption of NH_3 . *ACS Sustain. Chem. Eng.* **7**, 3258–3266 (2019). <https://doi.org/10.1021/acssuschemeng.8b05221>
62. F.-Y. Zhong, L. Zhou, J. Shen, Y. Liu, J.-P. Fan et al., Rational design of azole-based deep eutectic solvents for highly efficient and reversible capture of ammonia. *ACS Sustain. Chem. Eng.* **7**, 14170–14179 (2019). <https://doi.org/10.1021/acssuschemeng.9b02845>
63. Z.-L. Li, F.-Y. Zhong, J.-Y. Huang, H.-L. Peng, K. Huang, Sugar-based natural deep eutectic solvents as potential absorbents for NH_3 capture at elevated temperatures and reduced pressures. *J. Mol. Liq.* **317**, 113992 (2020). <https://doi.org/10.1016/j.molliq.2020.113992>
64. O.V. Kazarina, A.N. Petukhov, R.N. Nagrimanov, A.V. Vorotyntsev, M.E. Atlaskina et al., The role of HBA structure of deep eutectic solvents consisted of ethylene glycol and chlorides of a choline family for improving the ammonia capture performance. *J. Mol. Liq.* **373**, 121216 (2023). <https://doi.org/10.1016/j.molliq.2023.121216>
65. O.V. Kazarina, A.N. Petukhov, A.V. Vorotyntsev, M.E. Atlaskina, A.A. Atlaskin et al., The way for improving the efficiency of ammonia and carbon dioxide absorption of choline chloride: urea mixtures by modifying a choline cation. *Fluid Phase Equilib.* **568**, 113736 (2023). <https://doi.org/10.1016/j.fluid.2023.113736>
66. O.V. Kazarina, V.N. Agieienko, A.N. Petukhov, A.V. Vorotyntsev, M.E. Atlaskina et al., Deep eutectic solvents composed of urea and new salts of a choline family for efficient ammonia absorption. *J. Chem. Eng. Data* **67**, 138–150 (2022). <https://doi.org/10.1021/acs.jced.1c00684>
67. J.-Y. Zhang, K. Huang, Densities and viscosities of, and NH_3 solubilities in deep eutectic solvents composed of ethylamine



- hydrochloride and acetamide. *J. Chem. Thermodyn.* **139**, 105883 (2019). <https://doi.org/10.1016/j.jct.2019.105883>
68. W.-J. Jiang, F.-Y. Zhong, Y. Liu, K. Huang, Effective and reversible capture of NH_3 by ethylamine hydrochloride plus glycerol deep eutectic solvents. *ACS Sustain. Chem. Eng.* **7**, 10552–10560 (2019). <https://doi.org/10.1021/acssuschemeng.9b01102>
69. W.-J. Jiang, F.-Y. Zhong, L.-S. Zhou, H.-L. Peng, J.-P. Fan et al., Chemical dual-site capture of NH_3 by unprecedentedly low-viscosity deep eutectic solvents. *Chem. Commun.* **56**, 2399–2402 (2020). <https://doi.org/10.1039/C9CC09043F>
70. N.-N. Cheng, Z.-L. Li, H.-C. Lan, W.-L. Xu, W.-J. Jiang et al., Deep eutectic solvents with multiple weak acid sites for highly efficient, reversible and selective absorption of ammonia. *Sep. Purif. Technol.* **269**, 118791 (2021). <https://doi.org/10.1016/j.seppur.2021.118791>
71. L. Zheng, X. Zhang, Q. Li, Y. Ma, Z. Cai et al., Effective ammonia separation by non-chloride deep eutectic solvents composed of dihydroxybenzoic acids and ethylene glycol through multiple-site interaction. *Sep. Purif. Technol.* **309**, 123136 (2023). <https://doi.org/10.1016/j.seppur.2023.123136>
72. A.I. Akhmetshina, A.N. Petukhov, A. Mechergui, A.V. Vorotyntsev, A.V. Nyuchev et al., Evaluation of methanesulfonate-based deep eutectic solvent for ammonia sorption. *J. Chem. Eng. Data* **63**, 1896–1904 (2018). <https://doi.org/10.1021/acs.jced.7b01004>
73. Y. Cao, X. Zhang, S. Zeng, Y. Liu, H. Dong et al., Protic ionic liquid-based deep eutectic solvents with multiple hydrogen bonding sites for efficient absorption of NH_3 . *AIChE J.* **66**(8), e16253 (2020). <https://doi.org/10.1002/aic.16253>
74. Z.-L. Li, F.-Y. Zhong, L.-S. Zhou, Z.-Q. Tian, K. Huang, Deep eutectic solvents formed by N-methylacetamide and heterocyclic weak acids for highly efficient and reversible chemical absorption of ammonia. *Ind. Eng. Chem. Res.* **59**, 2060–2067 (2020). <https://doi.org/10.1021/acs.iecr.9b04924>
75. D. Deng, B. Gao, C. Zhang, X. Duan, Y. Cui et al., Investigation of protic NH_4SCN^- based deep eutectic solvents as highly efficient and reversible NH_3 absorbents. *Chem. Eng. J.* **358**, 936–943 (2019). <https://doi.org/10.1016/j.cej.2018.10.077>
76. D. Deng, X. Deng, X. Duan, L. Gong, Protic guanidine isothiocyanate plus acetamide deep eutectic solvents with low viscosity for efficient NH_3 capture and NH_3/CO_2 separation. *J. Mol. Liq.* **324**, 114719 (2021). <https://doi.org/10.1016/j.molliq.2020.114719>
77. B. Han, C. Butterly, W. Zhang, J.-Z. He, D. Chen, Adsorbent materials for ammonium and ammonia removal: a review. *J. Clean. Prod.* **283**, 124611 (2021). <https://doi.org/10.1016/j.jclepro.2020.124611>
78. N.Z. Mohd Azmi, A. Buthiyappan, A.A. Abdul Raman, M.F. Abdul Patah, S. Sufian, Recent advances in biomass based activated carbon for carbon dioxide capture—a review. *J. Ind. Eng. Chem.* **116**, 1–20 (2022). <https://doi.org/10.1016/j.jiec.2022.08.021>
79. F. Zhu, Z. Wang, J. Huang, W. Hu, D. Xie et al., Efficient adsorption of ammonia on activated carbon from hydrochar of pomelo peel at room temperature: role of chemical components in feedstock. *J. Clean. Prod.* **406**, 137076 (2023). <https://doi.org/10.1016/j.jclepro.2023.137076>
80. C. Cardenas, L. Sigot, C. Vallières, S. Marsteau, M. Marchal et al., Ammonia capture by adsorption on doped and undoped activated carbon: isotherm and breakthrough curve measurements. *Sep. Purif. Technol.* **313**, 123454 (2023). <https://doi.org/10.1016/j.seppur.2023.123454>
81. T. Zhang, H. Miyaoka, H. Miyaoka, T. Ichikawa, Y. Kojima, Review on ammonia absorption materials: metal hydrides, halides, and borohydrides. *ACS Appl. Energy Mater.* **1**, 232–242 (2018). <https://doi.org/10.1021/acsaem.7b00111>
82. J. Kim, H. Lee, H.T. Vo, G. Lee, N. Kim et al., Bead-shaped mesoporous alumina adsorbents for adsorption of ammonia. *Materials (Basel)* **13**, 1375 (2020). <https://doi.org/10.3390/ma13061375>
83. W. Zheng, J. Hu, S. Rappeport, Z. Zheng, Z. Wang et al., Activated carbon fiber composites for gas phase ammonia adsorption. *Microporous Mesoporous Mater.* **234**, 146–154 (2016). <https://doi.org/10.1016/j.micromeso.2016.07.011>
84. C. Li, S. Zhao, M. Li, Z. Yao, Y. Li et al., The effect of the active carbonyl groups and residual acid on the ammonia adsorption over the acid-modified activated carbon. *Front. Environ. Sci.* **11**, 976113 (2023). <https://doi.org/10.3389/fenvs.2023.976113>
85. W. Zhang, F. Liu, X. Kan, Y. Zheng, A. Zheng et al., Developing ordered mesoporous silica superacids for high-precision adsorption and separation of ammonia. *Chem. Eng. J.* **457**, 141263 (2023). <https://doi.org/10.1016/j.cej.2022.141263>
86. I. Matito-Martos, A. Martin-Calvo, C.O. Ania, J.B. Parra, J.M. Vicent-Luna et al., Role of hydrogen bonding in the capture and storage of ammonia in zeolites. *Chem. Eng. J.* **387**, 124062 (2020). <https://doi.org/10.1016/j.cej.2020.124062>
87. W. Ouyang, S. Zheng, C. Wu, X. Hu, R. Chen et al., Dynamic ammonia adsorption by FAU zeolites to below 0.1 ppm for hydrogen energy applications. *Int. J. Hydrog. Energy* **46**, 32559–32569 (2021). <https://doi.org/10.1016/j.ijhydene.2021.07.107>
88. J.M. Lucero, J.M. Crawford, C.A. Wolden, M.A. Carreon, Tunability of ammonia adsorption over NaP zeolite. *Microporous Mesoporous Mater.* **324**, 111288 (2021). <https://doi.org/10.1016/j.micromeso.2021.111288>
89. B. Zhakishva, J.J. Gutiérrez-Sevillano, S. Calero, Ammonia and water in zeolites: effect of aluminum distribution on the heat of adsorption. *Sep. Purif. Technol.* **306**, 122564 (2023). <https://doi.org/10.1016/j.seppur.2022.122564>
90. C. Shen, L. Shen, Cyclic NH_3 adsorption–desorption characteristics of Cu-based metal halides as ammonia separation and storage procedure. *J. Energy Inst.* **109**, 101250 (2023). <https://doi.org/10.1016/j.joei.2023.101250>
91. Z. Cao, F. Akhtar, Porous strontium chloride scaffolded by graphene networks as ammonia carriers. *Adv. Funct. Mater.* **31**, 2008505 (2021). <https://doi.org/10.1002/adfm.202008505>

92. T. Zhu, B. Pei, T. Di, Y. Xia, T. Li et al., Thirty-minute preparation of microporous polyimides with large surface areas for ammonia adsorption. *Green Chem.* **22**, 7003–7009 (2020). <https://doi.org/10.1039/d0gc02794d>
93. Y.-S. Han, S. An, J. Dai, J. Hu, Q. Xu et al., Defect-engineering of anionic porous aromatic frameworks for ammonia capture. *ACS Appl. Polym. Mater.* **3**, 4534–4542 (2021). <https://doi.org/10.1021/acsapm.1c00589>
94. J.F. Van Humbeck, T.M. McDonald, X. Jing, B.M. Wiers, G. Zhu et al., Ammonia capture in porous organic polymers densely functionalized with Brønsted acid groups. *J. Am. Chem. Soc.* **136**, 2432–2440 (2014). <https://doi.org/10.1021/ja4105478>
95. J. Zhang, Y. Ma, W. Wu, Z. Cai, Y. Cao et al., Carboxylic functionalized mesoporous polymers for fast, highly efficient, selective and reversible adsorption of ammonia. *Chem. Eng. J.* **448**, 137640 (2022). <https://doi.org/10.1016/j.cej.2022.137640>
96. D. Jung, Z. Chen, S. Alayoglu, M.R. Mian, T.A. Goetjen et al., Postsynthetically modified polymers of intrinsic microporosity (PIMs) for capturing toxic gases. *ACS Appl. Mater. Interfaces* **13**, 10409–10415 (2021). <https://doi.org/10.1021/acsami.0c21741>
97. C.-C. Hsieh, J.-S. Tsai, J.-R. Chang, Effects of moisture on NH₃ Capture using activated carbon and acidic porous polymer modified by impregnation with H₃PO₄: sorbent material characterized by synchrotron XRPD and FT-IR. *Materials (Basel)* **15**, 784 (2022). <https://doi.org/10.3390/ma15030784>
98. G. Barin, G.W. Peterson, V. Crocellà, J. Xu, K.A. Colwell et al., Highly effective ammonia removal in a series of Brønsted acidic porous polymers: investigation of chemical and structural variations. *Chem. Sci.* **8**, 4399–4409 (2017). <https://doi.org/10.1039/c6sc05079d>
99. Z. Han, Y. Mao, X. Pang, Y. Yan, Structure and functional group regulation of plastics for efficient ammonia capture. *J. Hazard. Mater.* **440**, 129789 (2022). <https://doi.org/10.1016/j.jhazmat.2022.129789>
100. J. Mi, W. Peng, Y. Luo, W. Chen, L. Lin et al., A cationic polymerization strategy to design sulfonated micro-mesoporous polymers as efficient adsorbents for ammonia capture and separation. *Macromolecules* **54**, 7010–7020 (2021). <https://doi.org/10.1021/acs.macromol.1c00376>
101. X. Kan, Z. Liu, F. Liu, F. Li, W. Chen et al., Sulfonated and ordered mesoporous polymers for reversible adsorption of ammonia: elucidation of sequential pore-space diffusion. *Chem. Eng. J.* **451**, 139085 (2023). <https://doi.org/10.1016/j.cej.2022.139085>
102. D.W. Kang, M. Kang, M. Moon, H. Kim, S. Eom et al., PDMS-coated hypercrosslinked porous organic polymers modified *via* double postsynthetic acidifications for ammonia capture. *Chem. Sci.* **9**, 6871–6877 (2018). <https://doi.org/10.1039/c8sc02640h>
103. D.W. Kang, M. Kang, D.W. Kim, H. Kim, Y.H. Lee et al., Engineered removal of trace NH₃ by porous organic polymers modified *via* sequential post-sulfonation and post-alkylation. *Adv. Sustain. Syst.* **5**, 2000161 (2021). <https://doi.org/10.1002/adsu.202000161>
104. R.J.S. Lima, D.V. Okhrimenko, S. Rudić, M.T.F. Telling, V.G. Sakai et al., Ammonia storage in hydrogen bond-rich microporous polymers. *ACS Appl. Mater. Interfaces* **12**, 58161–58169 (2020). <https://doi.org/10.1021/acsami.0c18855>
105. J.-W. Lee, G. Barin, G.W. Peterson, J. Xu, K.A. Colwell et al., A microporous amic acid polymer for enhanced ammonia capture. *ACS Appl. Mater. Interfaces* **9**, 33504–33510 (2017). <https://doi.org/10.1021/acsami.7b02603>
106. L. Luo, J. Li, X. Chen, X. Cao, Y. Liu et al., Superhigh and reversible NH₃ uptake of cobaltous thiocyanate functionalized porous poly ionic liquids through competitive and cooperative interactions. *Chem. Eng. J.* **427**, 131638 (2022). <https://doi.org/10.1016/j.cej.2021.131638>
107. L. Luo, Z. Wu, Z. Wu, Y. Liu, X. Huang et al., Role of structure in the ammonia uptake of porous polyionic liquids. *ACS Sustain. Chem. Eng.* **10**, 4094–4104 (2022). <https://doi.org/10.1021/acssuschemeng.1c06503>
108. D.W. Kang, S.E. Ju, D.W. Kim, M. Kang, H. Kim et al., Emerging porous materials and their composites for NH₃ gas removal. *Adv. Sci.* **7**, 2002142 (2020). <https://doi.org/10.1002/adv.202002142>
109. M.-S. Yao, W.-H. Li, G. Xu, Metal–organic frameworks and their derivatives for electrically-transduced gas sensors. *Coord. Chem. Rev.* **426**, 213479 (2021). <https://doi.org/10.1016/j.ccr.2020.213479>
110. M.-S. Yao, K.-I. Otake, J. Zheng, M. Tsujimoto, Y.-F. Gu et al., Integrated soft porosity and electrical properties of conductive-on-insulating metal–organic framework nanocrystals. *Angew. Chem. Int. Ed.* **62**, e202303903 (2023). <https://doi.org/10.1002/anie.202303903>
111. Y. Gao, J. Wang, Y. Yang, J. Wang, C. Zhang et al., Engineering spin states of isolated copper species in a metal–organic framework improves urea electrosynthesis. *Nano-Micro Lett.* **15**, 158 (2023). <https://doi.org/10.1007/s40820-023-01127-0>
112. C. Li, Y. Ji, Y. Wang, C. Liu, Z. Chen et al., Applications of metal–organic frameworks and their derivatives in electrochemical CO₂ reduction. *Nano-Micro Lett.* **15**, 113 (2023). <https://doi.org/10.1007/s40820-023-01092-8>
113. A. Takahashi, H. Tanaka, D. Parajuli, T. Nakamura, K. Minami et al., Historical pigment exhibiting ammonia gas capture beyond standard adsorbents with adsorption sites of two kinds. *J. Am. Chem. Soc.* **138**, 6376–6379 (2016). <https://doi.org/10.1021/jacs.6b02721>
114. A.J. Rieth, M. Dincă, Controlled gas uptake in metal–organic frameworks with record ammonia sorption. *J. Am. Chem. Soc.* **140**, 3461–3466 (2018). <https://doi.org/10.1021/jacs.8b00313>
115. A. Carné-Sánchez, J. Martínez-Esaín, T. Rookard, C.J. Flood, J. Farauto et al., Ammonia capture in rhodium(II)-based metal–organic polyhedra *via* synergistic coordinative and H-bonding interactions. *ACS Appl. Mater. Interfaces* **15**, 6747–6754 (2023). <https://doi.org/10.1021/acsami.2c19206>



116. D. Zhang, Y. Shen, J. Ding, H. Zhou, Y. Zhang et al., Tunable ammonia adsorption within metal–organic frameworks with different unsaturated metal sites. *Molecules* **27**, 7847 (2022). <https://doi.org/10.3390/molecules27227847>
117. S. Moribe, Z. Chen, S. Alayoglu, Z.H. Syed, T. Islamoglu et al., Ammonia capture within isoreticular metal–organic frameworks with rod secondary building units. *ACS Mater. Lett.* **1**, 476–480 (2019). <https://doi.org/10.1021/acsmaterialslett.9b00307>
118. K.O. Kirlikovali, Z. Chen, X. Wang, M.R. Mian, S. Alayoglu et al., Investigating the influence of hexanuclear clusters in isostructural metal–organic frameworks on toxic gas adsorption. *ACS Appl. Mater. Interfaces* **14**, 3048–3056 (2022). <https://doi.org/10.1021/acsami.1c20518>
119. D.W. Kim, D.W. Kang, M. Kang, J.H. Lee, J.H. Choe et al., High ammonia uptake of a metal–organic framework adsorbent in a wide pressure range. *Angew. Chem. Int. Ed.* **59**, 22531–22536 (2020). <https://doi.org/10.1002/anie.202012552>
120. T.N. Nguyen, I.M. Harreschou, J.-H. Lee, K.C. Stylianou, D.W. Stephan, A recyclable metal–organic framework for ammonia vapour adsorption. *Chem. Commun.* **56**, 9600–9603 (2020). <https://doi.org/10.1039/d0cc00741b>
121. C. Marsh, X. Han, J. Li, Z. Lu, S.P. Argent et al., Exceptional packing density of ammonia in a dual-functionalized metal–organic framework. *J. Am. Chem. Soc.* **143**, 6586–6592 (2021). <https://doi.org/10.1021/jacs.1c01749>
122. Z. Fang, B. Bueken, D.E. De Vos, R.A. Fischer, Defect-engineered metal–organic frameworks. *Angew. Chem. Int. Ed.* **54**, 7234–7254 (2015). <https://doi.org/10.1002/anie.201411540>
123. J. Ren, M. Ledwaba, N.M. Musyoka, H.W. Langmi, M. Mathe et al., Structural defects in metal–organic frameworks (MOFs): formation, detection and control towards practices of interests. *Coord. Chem. Rev.* **349**, 169–197 (2017). <https://doi.org/10.1016/j.ccr.2017.08.017>
124. Q.-Y. Ju, J.-J. Zheng, L. Xu, H.-Y. Jiang, Z.-Q. Xue et al., Enhanced carbon capture with motif-rich amino acid loaded defective robust metal–organic frameworks. *Nano Res.* **17**, 2004–2010 (2024). <https://doi.org/10.1007/s12274-023-5961-y>
125. Y. Ma, W. Lu, X. Han, Y. Chen, I. da Silva et al., Direct observation of ammonia storage in UiO-66 incorporating Cu(II) binding sites. *J. Am. Chem. Soc.* **144**, 8624–8632 (2022). <https://doi.org/10.1021/jacs.2c00952>
126. G.W. Peterson, G.W. Wagner, A. Balboa, J. Mahle, T. Sewell et al., Ammonia vapor removal by Cu(3)(BTC)(2) and its characterization by MAS NMR. *J. Phys. Chem. C Nanomater. Interfaces* **113**, 13906–13917 (2009). <https://doi.org/10.1021/jp902736z>
127. C. Bae, M. Gu, Y. Jeon, D. Kim, J. Kim, Metal–organic frameworks for NH₃ adsorption by different NH₃ operating pressures. *Bull. Korean Chem. Soc.* **44**(2), 112–124 (2022). <https://doi.org/10.1002/bkcs.12640>
128. J.H. Carter, C.G. Morris, H.G.W. Godfrey, S.J. Day, J. Potter et al., Long-term stability of MFM-300(Al) toward toxic air pollutants. *ACS Appl. Mater. Interfaces* **12**, 42949–42954 (2020). <https://doi.org/10.1021/acsami.0c11134>
129. H.G.W. Godfrey, I. da Silva, L. Briggs, J.H. Carter, C.G. Morris et al., Ammonia storage by reversible host-guest site exchange in a robust metal–organic framework. *Angew. Chem. Int. Ed.* **57**, 14778–14781 (2018). <https://doi.org/10.1002/anie.201808316>
130. X. Han, W. Lu, Y. Chen, I. da Silva, J. Li et al., High ammonia adsorption in MFM-300 materials: dynamics and charge transfer in host-guest binding. *J. Am. Chem. Soc.* **143**, 3153–3161 (2021). <https://doi.org/10.1021/jacs.0c11930>
131. Z. Wang, Z. Li, H. Wang, Y. Zhao, Q. Xia et al., Regulating the pore microenvironment of microporous metal–organic frameworks for efficient adsorption of low-concentration ammonia. *ACS Sustain. Chem. Eng.* **10**, 10945–10954 (2022). <https://doi.org/10.1021/acssuschemeng.2c02944>
132. J.H. Lee, S. Jeoung, Y.G. Chung, H.R. Moon, Elucidation of flexible metal–organic frameworks: research progresses and recent developments. *Coord. Chem. Rev.* **389**, 161–188 (2019). <https://doi.org/10.1016/j.ccr.2019.03.008>
133. I. Senkovska, V. Bon, L. Abylgazina, M. Mendt, J. Berger et al., Understanding MOF flexibility: an analysis focused on pillared layer MOFs as a model system. *Angew. Chem. Int. Ed.* **62**, e202218076 (2023). <https://doi.org/10.1002/anie.202218076>
134. Y. Chen, B. Shan, C. Yang, J. Yang, J. Li et al., Environmentally friendly synthesis of flexible MOFs M(NA)₂ (M = Zn, Co, Cu, Cd) with large and regenerable ammonia capacity. *J. Mater. Chem. A* **6**, 9922–9929 (2018). <https://doi.org/10.1039/C8TA02845A>
135. D.W. Kang, M. Kang, H. Kim, J.H. Choe, D.W. Kim et al., A hydrogen-bonded organic framework (HOF) with type IV NH₃ adsorption behavior. *Angew. Chem. Int. Ed.* **58**, 16152–16155 (2019). <https://doi.org/10.1002/anie.201911087>
136. X. Song, Y. Wang, C. Wang, X. Gao, Y. Zhou et al., Self-healing hydrogen-bonded organic frameworks for low-concentration ammonia capture. *J. Am. Chem. Soc.* **146**, 627–634 (2024). <https://doi.org/10.1021/jacs.3c10492>
137. J. Li, L. Luo, L. Yang, C. Zhao, Y. Liu et al., Ionic framework constructed with protic ionic liquid units for improving ammonia uptake. *Chem. Commun.* **57**, 4384–4387 (2021). <https://doi.org/10.1039/d1cc00441g>
138. C.J. Doonan, D.J. Tranchemontagne, T.G. Glover, J.R. Hunt, O.M. Yaghi, Exceptional ammonia uptake by a covalent organic framework. *Nat. Chem.* **2**, 235–238 (2010). <https://doi.org/10.1038/nchem.548>
139. Y. Cao, R. Wu, Y.-Y. Gao, Y. Zhou, J.-J. Zhu, Advances of electrochemical and electrochemiluminescent sensors based on covalent organic frameworks. *Nano-Micro Lett.* **16**, 37 (2023). <https://doi.org/10.1007/s40820-023-01249-5>
140. Y. Yang, M. Faheem, L. Wang, Q. Meng, H. Sha et al., Surface pore engineering of covalent organic frameworks for ammonia capture through synergistic multivariate and open metal site approaches. *ACS Cent. Sci.* **4**, 748–754 (2018). <https://doi.org/10.1021/acscentsci.8b00232>

141. Y. Zhao, S. Zhang, L. Wu, C. Guo, X. Song, Multiscale study on ammonia adsorption by Li-doped COF-10. *Comput. Theor. Chem.* **1175**, 112744 (2020). <https://doi.org/10.1016/j.comptc.2020.112744>
142. Z. Zhu, H. Wang, X.-Y. Wu, K. Luo, J. Fan, Computational screening of metal–organic frameworks for ammonia capture from H₂/N₂/NH₃ mixtures. *ACS Omega* **7**, 37640–37653 (2022). <https://doi.org/10.1021/acsomega.2c04517>
143. Y. Khabzina, D. Farrusseng, Unravelling ammonia adsorption mechanisms of adsorbents in humid conditions. *Microporous Mesoporous Mater.* **265**, 143–148 (2018). <https://doi.org/10.1016/j.micromeso.2018.02.011>
144. R. Chen, J. Liu, Competitive coadsorption of ammonia with water and sulfur dioxide on metal–organic frameworks at low pressure. *Build. Environ.* **207**, 108421 (2022). <https://doi.org/10.1016/j.buildenv.2021.108421>
145. C. Shen, P. Wang, L. Shen, X. Yin, Z. Miao, NH₃ adsorption performance of silicon-supported metal chlorides. *Ind. Eng. Chem. Res.* **61**, 8616–8623 (2022). <https://doi.org/10.1021/acs.iecr.2c00916>
146. C. Shen, L. Shen, XCl₂/MWCNTs—Composites based on multi-walled carbon nanotubes and metal chlorides for NH₃ capture and separation. *Energy Fuels* **37**, 5995–6001 (2023). <https://doi.org/10.1021/acs.energyfuels.3c00467>
147. X. Tian, J. Qiu, Z. Wang, Y. Chen, Z. Li et al., A record ammonia adsorption by calcium chloride confined in covalent organic frameworks. *Chem. Commun.* **58**, 1151–1154 (2022). <https://doi.org/10.1039/D1CC06308A>
148. Y. Jian, W. Hu, Z. Zhao, P. Cheng, H. Haick et al., Gas sensors based on chemi-resistive hybrid functional nanomaterials. *Nano-Micro Lett.* **12**, 71 (2020). <https://doi.org/10.1007/s40820-020-0407-5>
149. K.N. Ruckart, Y. Zhang, W.M. Reichert, G.W. Peterson, T.G. Glover, Sorption of ammonia in mesoporous-silica ionic liquid composites. *Ind. Eng. Chem. Res.* **55**, 12191–12204 (2016). <https://doi.org/10.1021/acs.iecr.6b02041>
150. A. Kaftan, H. Klefer, M. Haumann, M. Laurin, P. Wasserscheid et al., An operando DRIFTS-MS study of NH₃ removal by supported ionic liquid phase (SILP) materials. *Sep. Purif. Technol.* **174**, 245–250 (2017). <https://doi.org/10.1016/j.seppur.2016.10.017>
151. M. Yu, S. Zeng, Z. Wang, Z. Hu, H. Dong et al., Protic ionic-liquid-supported activated carbon with hierarchical pores for efficient NH₃ adsorption. *ACS Sustain. Chem. Eng.* **7**, 11769–11777 (2019). <https://doi.org/10.1021/acssuschemeng.9b02051>
152. Y. Li, S. Zeng, S. Zheng, T. Zhao, X. Sun et al., Mesoporous multiproton ionic liquid hybrid adsorbents for facilitating NH₃ separation. *Ind. Eng. Chem. Res.* **62**, 2829–2842 (2023). <https://doi.org/10.1021/acs.iecr.2c03193>
153. S. Zheng, Q. Xu, S. Zeng, G. Li, H. Jiang et al., Porous multi-site ionic liquid composites for superior selective and reversible adsorption of ammonia. *Sep. Purif. Technol.* **310**, 123161 (2023). <https://doi.org/10.1016/j.seppur.2023.123161>
154. D. Cao, Z. Li, Z. Wang, H. Wang, S. Gao et al., Highly dispersed ionic liquids in mesoporous molecular sieves enable a record NH₃ absorption. *ACS Sustain. Chem. Eng.* **9**, 16363–16372 (2021). <https://doi.org/10.1021/acssuschemeng.1c06151>
155. S. Zeng, J. Wang, P. Li, H. Dong, H. Wang et al., Efficient adsorption of ammonia by incorporation of metal ionic liquids into silica gels as mesoporous composites. *Chem. Eng. J.* **370**, 81–88 (2019). <https://doi.org/10.1016/j.cej.2019.03.180>
156. G. Han, C. Liu, Q. Yang, D. Liu, C. Zhong, Construction of stable IL@MOF composite with multiple adsorption sites for efficient ammonia capture from dry and humid conditions. *Chem. Eng. J.* **401**, 126106 (2020). <https://doi.org/10.1016/j.cej.2020.126106>
157. G. Han, F. Li, M. Guo, H. Fan, Q. Guo et al., MIL-101(Cr) loaded simple ILs for efficient ammonia capture and selective separation. *Chem. Eng. J.* **471**, 144545 (2023). <https://doi.org/10.1016/j.cej.2023.144545>
158. Y. Shi, Z. Wang, Z. Li, H. Wang, D. Xiong et al., Anchoring LiCl in the nanopores of metal–organic frameworks for ultra-high uptake and selective separation of ammonia. *Angew. Chem. Int. Ed.* **61**, e202212032 (2022). <https://doi.org/10.1002/anie.202212032>
159. Q. Luo, E. Pentzer, Encapsulation of ionic liquids for tailored applications. *ACS Appl. Mater. Interfaces* **12**, 5169–5176 (2020). <https://doi.org/10.1021/acsami.9b16546>
160. R. Santiago, J. Lemus, D. Moreno, C. Moya, M. Larriba et al., From kinetics to equilibrium control in CO₂ capture columns using Encapsulated Ionic Liquids (ENILs). *Chem. Eng. J.* **348**, 661–668 (2018). <https://doi.org/10.1016/j.cej.2018.05.029>
161. S. Zheng, S. Zeng, Y. Li, L. Bai, Y. Bai et al., State of the art of ionic liquid-modified adsorbents for CO₂ capture and separation. *AIChE J.* **68**, e17500 (2022). <https://doi.org/10.1002/aic.17500>
162. J. Palomar, J. Lemus, N. Alonso-Morales, J. Bedia, M.A. Gilarranz et al., Encapsulated ionic liquids (ENILs): from continuous to discrete liquid phase. *Chem. Commun.* **48**, 10046–10048 (2012). <https://doi.org/10.1039/C2CC35291E>
163. J. Lemus, J. Bedia, C. Moya, N. Alonso-Morales, M.A. Gilarranz et al., Ammonia capture from the gas phase by encapsulated ionic liquids (ENILs). *RSC Adv.* **6**, 61650–61660 (2016). <https://doi.org/10.1039/C6RA11685J>
164. N. O'Reilly, N. Giri, S.L. James, Porous liquids. *Chem. Eur. J.* **13**(11), 3020–3025 (2007). <https://doi.org/10.1002/chem.200700090>
165. N. Giri, M.G. Del Pópolo, G. Melaugh, R.L. Greenaway, K. Rätzke et al., Liquids with permanent porosity. *Nature* **527**, 216–220 (2015). <https://doi.org/10.1038/nature16072>
166. K. Jie, Y. Zhou, H.P. Ryan, S. Dai, J.R. Nitschke, Engineering permanent porosity into liquids. *Adv. Mater.* **33**, 2005745 (2021). <https://doi.org/10.1002/adma.202005745>
167. J. Zhang, S.-H. Chai, Z.-A. Qiao, S.M. Mahurin, J. Chen et al., Porous liquids: a promising class of media for gas separation. *Angew. Chem. Int. Ed.* **54**, 932–936 (2015). <https://doi.org/10.1002/anie.201409420>



168. W. Shan, P.F. Fulvio, L. Kong, J.A. Schott, C.-L. Do-Thanh et al., New class of type III porous liquids: a promising platform for rational adjustment of gas sorption behavior. *ACS Appl. Mater. Interfaces* **10**, 32–36 (2018). <https://doi.org/10.1021/acsami.7b15873>
169. B.D. Egleston, K.V. Luzyanin, M.C. Brand, R. Clowes, M.E. Briggs et al., Controlling gas selectivity in molecular porous liquids by tuning the cage window size. *Angew. Chem. Int. Ed.* **59**, 7362–7366 (2020). <https://doi.org/10.1002/anie.201914037>
170. D.P. Erdosy, M.B. Wenny, J. Cho, C. DelRe, M.V. Walter et al., Microporous water with high gas solubilities. *Nature* **608**, 712–718 (2022). <https://doi.org/10.1038/s41586-022-05029-w>
171. N. Giri, C.E. Davidson, G. Melaugh, M.G. Del Pópolo, J.T.A. Jones et al., Alkylated organic cages: from porous crystals to neat liquids. *Chem. Sci.* **3**, 2153 (2012). <https://doi.org/10.1039/c2sc01007k>
172. T.D. Bennett, F.-X. Coudert, S.L. James, A.I. Cooper, The changing state of porous materials. *Nat. Mater.* **20**, 1179–1187 (2021). <https://doi.org/10.1038/s41563-021-00957-w>
173. R. Gaillac, P. Pullumbi, K.A. Beyer, K.W. Chapman, D.A. Keen et al., Liquid metal–organic frameworks. *Nat. Mater.* **16**, 1149–1154 (2017). <https://doi.org/10.1038/nmat4998>
174. S. Liu, J. Liu, X. Hou, T. Xu, J. Tong et al., Porous liquid: a stable ZIF-8 colloid in ionic liquid with permanent porosity. *Langmuir* **34**, 3654–3660 (2018). <https://doi.org/10.1021/acs.langmuir.7b04212>
175. D.S. Sholl, R.P. Lively, Seven chemical separations to change the world. *Nature* **532**, 435–437 (2016). <https://doi.org/10.1038/532435a>
176. D.L. Gin, R.D. Noble, Designing the next generation of chemical separation membranes. *Science* **332**, 674–676 (2011). <https://doi.org/10.1126/science.1203771>
177. H. Wang, J. Zhao, Y. Li, Y. Cao, Z. Zhu et al., Aqueous two-phase interfacial assembly of COF membranes for water desalination. *Nano-Micro Lett.* **14**, 216 (2022). <https://doi.org/10.1007/s40820-022-00968-5>
178. I.V. Vorotyntsev, P.N. Drozdov, N.V. Karyakin, Ammonia permeability of a cellulose acetate membrane. *Inorg. Mater.* **42**, 231–235 (2006). <https://doi.org/10.1134/S0020168506030034>
179. C. Makhloufi, D. Roizard, E. Favre, Reverse selective NH₃/CO₂ permeation in fluorinated polymers using membrane gas separation. *J. Membr. Sci.* **441**, 63–72 (2013). <https://doi.org/10.1016/j.memsci.2013.03.048>
180. A.V. Vorobiev, I.N. Beckman, Ammonia and carbon dioxide permeability through perfluorosulfonic membranes. *Russ. Chem. Bull.* **51**, 275–281 (2002). <https://doi.org/10.1023/A:1015403626398>
181. W.A. Phillip, E. Martono, L. Chen, M.A. Hillmyer, E.L. Cussler, Seeking an ammonia selective membrane based on nanostructured sulfonated block copolymers. *J. Membr. Sci.* **337**, 39–46 (2009). <https://doi.org/10.1016/j.memsci.2009.03.013>
182. L. Ansaloni, Z. Dai, J.J. Ryan, K.P. Mineart, Q. Yu et al., Solvent-templated Block ionomers for base- and acid-gas separations: effect of humidity on ammonia and carbon dioxide permeation. *Adv. Mater. Interfaces* **4**, 1700854 (2017). <https://doi.org/10.1002/admi.201700854>
183. K. Wakimoto, W.-W. Yan, N. Moriyama, H. Nagasawa, M. Kanezashi et al., Ammonia permeation of fluorinated sulfonic acid polymer/ceramic composite membranes. *J. Membr. Sci.* **658**, 120718 (2022). <https://doi.org/10.1016/j.memsci.2022.120718>
184. B. Yang, L. Bai, Z. Wang, H. Jiang, S. Zeng et al., Exploring NH₃ transport properties by tailoring ionic liquids in Pebax-based hybrid membranes. *Ind. Eng. Chem. Res.* **60**, 9570–9577 (2021). <https://doi.org/10.1021/acs.iecr.1c01408>
185. H. Jiang, L. Bai, K. Peng, L. Yuan, S. Zheng et al., Blended membranes with ionic liquids tailoring by hydroxyl group for efficient NH₃ separation. *J. Membr. Sci.* **674**, 121480 (2023). <https://doi.org/10.1016/j.memsci.2023.121480>
186. B. Yang, L. Bai, T. Li, L. Deng, L. Liu et al., Super selective ammonia separation through multiple-site interaction with ionic liquid-based hybrid membranes. *J. Membr. Sci.* **628**, 119264 (2021). <https://doi.org/10.1016/j.memsci.2021.119264>
187. B. Yang, L. Bai, S. Zeng, S. Luo, L. Liu et al., NH₃ separation membranes with self-assembled gas highways induced by protic ionic liquids. *Chem. Eng. J.* **421**, 127876 (2021). <https://doi.org/10.1016/j.cej.2020.127876>
188. Z. Wang, H. Dong, X. Yu, Y. Ji, T. Hou et al., Two-dimensional porous polyphthalocyanine (PPc) as an efficient gas-separation membrane for ammonia synthesis. *Curr. Appl. Phys.* **17**, 1765–1770 (2017). <https://doi.org/10.1016/j.cap.2017.08.019>
189. I.I. Zaripov, I.M. Davletbaeva, Z.Z. Faizulina, R.S. Davletbaev, A.T. Gubaidullin et al., Synthesis and characterization of novel nanoporous gl-POSS-branched polymeric gas separation membranes. *Membranes* **10**, 110 (2020). <https://doi.org/10.3390/membranes10050110>
190. M. Kanezashi, A. Yamamoto, T. Yoshioka, T. Tsuru, Characteristics of ammonia permeation through porous silica membranes. *AIChE. J.* **56**, 1204–1212 (2010). <https://doi.org/10.1002/aic.12059>
191. O. Camus, S. Perera, B. Crittenden, Y.C. van Delft, D.F. Meyer et al., Ceramic membranes for ammonia recovery. *AIChE. J.* **52**, 2055–2065 (2006). <https://doi.org/10.1002/aic.10800>
192. H. Inami, C. Abe, Y. Hasegawa, Development of ammonia selectively permeable zeolite membrane for sensor in sewer system. *Membranes* **11**, 348 (2021). <https://doi.org/10.3390/membranes11050348>
193. D.I. Petukhov, A.S. Kan, A.P. Chumakov, O.V. Konovalov, R.G. Valeev et al., MXene-based gas separation membranes with sorption type selectivity. *J. Membr. Sci.* **621**, 118994 (2021). <https://doi.org/10.1016/j.memsci.2020.118994>
194. M.A. Komkova, I.S. Sadilov, V.A. Brotsman, D.I. Petukhov, A.A. Eliseev, Facilitated transport of ammonia in ultra-thin

- Prussian Blue membranes with potential-tuned selectivity. *J. Membr. Sci.* **639**, 119714 (2021). <https://doi.org/10.1016/j.memsci.2021.119714>
195. Q. Wei, J.M. Lucero, J.M. Crawford, J.D. Way, C.A. Wolden et al., Ammonia separation from N_2 and H_2 over LTA zeolitic imidazolate framework membranes. *J. Membr. Sci.* **623**, 119078 (2021). <https://doi.org/10.1016/j.memsci.2021.119078>
196. S. Padinjarekutt, H. Li, S. Ren, P. Ramesh, F. Zhou et al., Na^+ -gated nanochannel membrane for highly selective ammonia (NH_3) separation in the Haber-Bosch process. *Chem. Eng. J.* **454**, 139998 (2023). <https://doi.org/10.1016/j.cej.2022.139998>
197. S. Padinjarekutt, B. Sengupta, H. Li, K. Friedman, D. Behera et al., Synthesis of Na^+ -gated nanochannel membranes for the ammonia (NH_3) separation. *J. Membr. Sci.* **674**, 121512 (2023). <https://doi.org/10.1016/j.memsci.2023.121512>
198. L. Yu, L. Hao, Y. Feng, J. Pang, M. Guo et al., Assembling ionic liquid into porous molecular filler of mixed matrix membrane to trigger high gas permeability, selectivity, and stability for CO_2/CH_4 separation. *Nano Res.* **17**, 4535–4543 (2024). <https://doi.org/10.1007/s12274-023-6329-z>
199. Y. Wang, Y. Ren, Y. Cao, X. Liang, G. He et al., Engineering HOF-based mixed-matrix membranes for efficient CO_2 separation. *Nano-Micro Lett.* **15**, 50 (2023). <https://doi.org/10.1007/s40820-023-01020-w>
200. Y. Yang, B. Pang, W. Zeng, B. Ma, P. Yin et al., Enhance gas-separation efficiency of mixed matrix membranes by lamellarly arranged metal–organic polyhedron. *Nano Res.* **16**, 11450–11454 (2023). <https://doi.org/10.1007/s12274-023-5874-9>
201. A. Raza, S. Farrukh, A. Hussain, Synthesis, characterization and NH_3/N_2 gas permeation study of nanocomposite membranes. *J. Polym. Environ.* **25**, 46–55 (2017). <https://doi.org/10.1007/s10924-016-0783-6>
202. J.B. DeCoste, M.S. Denny Jr., G.W. Peterson, J.J. Mahle, S.M. Cohen, Enhanced aging properties of HKUST-1 in hydrophobic mixed-matrix membranes for ammonia adsorption. *Chem. Sci.* **7**, 2711–2716 (2016). <https://doi.org/10.1039/c5sc04368a>
203. H. Jiang, L. Bai, Z. Wang, W. Zheng, B. Yang et al., Mixed matrix membranes containing Cu-based metal organic framework and functionalized ionic liquid for efficient NH_3 separation. *J. Membr. Sci.* **659**, 120780 (2022). <https://doi.org/10.1016/j.memsci.2022.120780>
204. M.-S. Yao, K.-I. Otake, T. Koganezawa, M. Ogasawara, H. Asakawa et al., Growth mechanisms and anisotropic softness–dependent conductivity of orientation-controllable metal–organic framework nanofilms. *Proc. Natl. Acad. Sci. U.S.A.* **120**, e2305125120 (2023). <https://doi.org/10.1073/pnas.2305125120>
205. M.-S. Yao, K.-I. Otake, S. Kitagawa, Interface chemistry of conductive crystalline porous thin films. *Trends Chem.* **5**, 588–604 (2023). <https://doi.org/10.1016/j.trechm.2023.03.002>

